Galactic Gravitational Microlensing

A tool to detect low-mass extrasolar planets with potential application to the SONG telescope network

Basic concepts of microlensing and outline of an early-alert system based on available data from sky survey monitoring programs

---

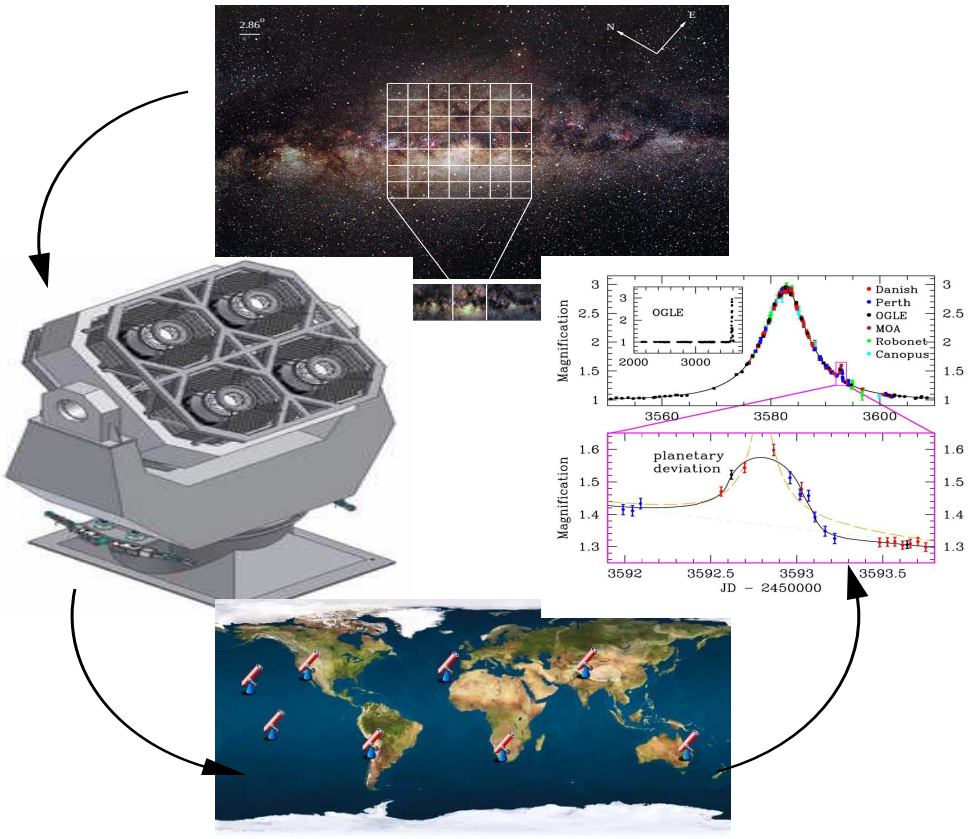

Applicant:	Uffe Gråe Jørgensen	(uffegj@nbi.dk)
Research assistant:	Tobias Cornelius Hinse	(tobiash@astro.ku.dk)

06.December 2006

Table of Contents

Chapter 1

Introduction and report outline

The existence of planets outside the solar system have been confirmed since the first announcement of an extrasolar planet by Mayor and Queloz (1995). Currently (December 2006) the total number of planets detected around other stars counts 209 with an increasing tendency each year. Different methods for their observation and detection are employed. The most used method for observing extrasolar planets is the radial velocity technique based on the Doppler effect. This technique inferres the presence of an orbiting planet indirectly by measuring the induced reflex motion of the host star by the planet. Accounting for nearly 94 % of the total number of observed planets, the radial velocity technique is most sensitive in the detection of massive, close-in planets. A substantial part of the observed planet population are comparable in mass with Jupiter orbiting their host star on close-in orbits.

In order to detect low-mass planets with similar orbital characteristics as the terrestrial planets within the solar system, other techniques are available for astronomical observations. A preferred method suitable for the detection of low-mass planets is the so-called gravitational microlensing technique. In particular, this technique is capable of detecting Earth-like planets (with masses $1 - 10\ M_{\oplus}$) at distances around ~ 1 AU and larger.

The observation of the gravitational microlensing effect is based on standard differential photometry and takes advantage of a magnification event of a background field star (source) caused by the gravitational field of a lens star. The amount of magnification depends on the alignment of the observer, the lens star (possibly harbouring a planet) and the magnified background field star. The duration of a microlensing event is on the order of a few to several weeks. The presence of a planet introduces an extra gravitational field in addition to the gravitational field of the lens star. This effect is observed in a systematic deviation (or several deviations) within the light curve. Timescale for the duration of the deviation are on the order of hours (for Earth-mass planets) to days (for Jupiter-mass planets). Within a follow-up observation program, a dense time sampling of the ongoing microlensing event is important in order to cover

any possible deviations that might indicate the presence of a planet. For objects with V-band magnitude in the range 19 - 22 mag, this deviating effect is easily detected with a present day ground based 1-meter-class telescope. Several international collaboration projects are currently involved in the search for extrasolar planets (PLANET, MicroFUN, etc.) and extensive follow-up observations of selected microlensing events are conducted to detect possible photometric deviation(s) within the observed light curve. A vital component in detecting extrasolar planets, based on the microlensing

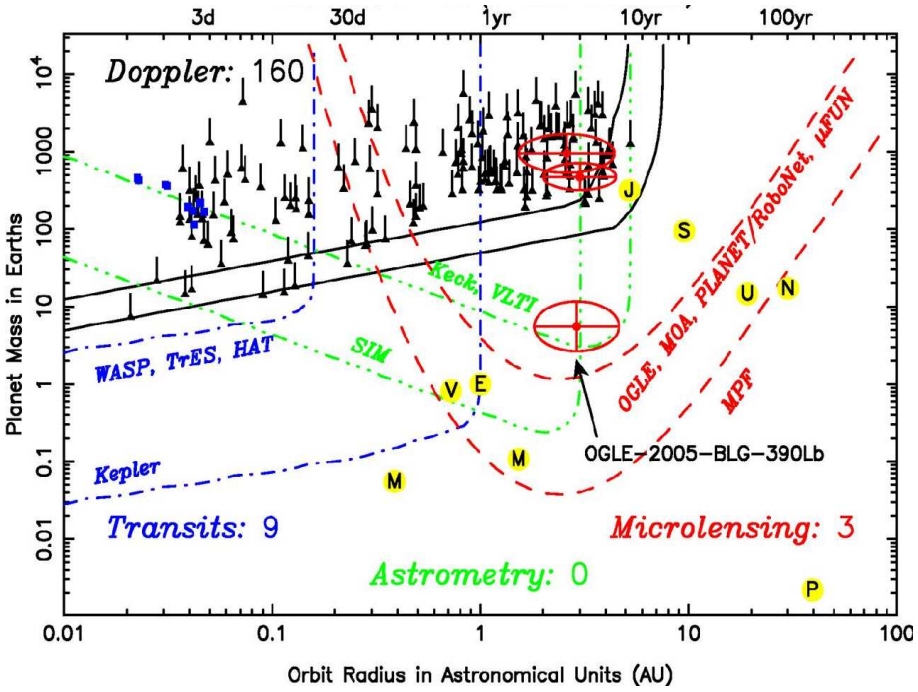

Figure 1.1: Different planet detection techniques and their sensitivity regime within mass-distance space.

method, is the availability of a large number of microlensing candidates for subsequent follow-up observations. The existence of a planet in orbit around the lens star is not always revealed within the observed light curve and the detection of planet anomalies is highly dependent on the relative motion between the background field star and the lens star on the sky. The planet detection probability increases for near alignment configurations between the observer, the lens star and the background field star; resulting in a brightness increase for the source star. In general, well suited microlensing events are characterised by *high-magnification* light curves.

In principle, stellar microlensing events in our Galaxy could be predicted from simple Newtonian mechanics, if all stars and their movement on the sky were known. In practice, however, the position and movement of only a fraction of the stars in our

Galaxy are known, and predicting the beginning of an microlensing event from known stellar movements is therefore not possible. Often, one of the components (the lensing star) is too faint in order to be resolved with current telescope technology (roughly, the lens- and source star are located within 1 pixel on the CCD). Therefore, it is necessary to frequently monitor a large number of star fields to infer and detect a brightness change associated with the characteristics of the beginning of an microlensing event. Large microlensing monitoring programs were initiated with the aim of using the detection of microlensing events to give us statistical information on the Galactic properties, such as the stellar mass function, the number of compact objects, brown dwarfs and the mass of the Galaxy.

Dedicated follow-up observing programs heavily rely on observations and results from large-scale monitoring surveys (OGLE, MOA) of selected star fields. In order to increase the chance of observing the onset of a microlensing event observation and monitoring programs are mainly directed and conducted around the galactic center within the galactic plane. The successful detection of microlensing events is issued by an early-alert announcement to the follow-up observation collaboration community (PLANET, MicroFUN). At current time, a total of 4 extrasolar planets have been detected by gravitational microlensing.

Increasing the detection rate of extrasolar planets requires an increase in the detection rate of microlensing events. If more microlensing events are available the more well suited high-amplification events can be chosen from the observed candidates for the compilation of a follow-up observing target list. A method to increase the detection rate of microlensing events is the use and analysis of public domain astronomical data obtained from current and future planned large-scale sky survey monitoring programs. High-speed Internet connections make easy access to publicly (or private) available astronomical databases a reality. The advent of extensive data storing, filing and exchange using the Internet has opened a new dimension in astronomical data retrieval, processing and analysis in order to probe the near universe for existing and new phenomena. In the future, astronomical and astrophysical science relies on the analysis of huge data volumes (on the order of Tera- to Peta bytes) and is generally associated with sky survey (monitoring) projects. The most well known projects indicating this change in the scale of astronomical data sets are the Sloan Digital Sky Survey[1] and the 2MASS[2] infrared survey. New technology in computer hardware (storing capabilities and processing power) and telescope design (large aperture mirrors and large format CCD cameras) made it possible to initiate and conduct such sky survey projects.

In the future, more ambitious survey projects are planned to frequently monitor star fields within systematic all-sky survey programs. The scientific main objective for initiating such survey programs ranges from the detection of Near-Earth Objects within

[1] http://www.sdss.org

[2] http://irsa.ipac.caltech.edu

the solar system to the observation of variable young stellar objects embedded within nearby star formation regions. On-line archives holding astronomical photometric data as a result from sky survey projects hold valuable information waiting for further mining, extraction and interpretation. An important spin-off activity of scientific value based on sky survey and monitoring projects, is the observation of transient and short-lived astronomical phenomena detected as individual variable objects. Examples are: microlensing events, gamma-ray bursts, supernovae, eclipsing binary, etc..

A successful realisation for extracting useful data products aiming at the detection of microlensing events includes the design of optimal data handling and search routines within the survey imaging data archive. Designing a data retrieval and analysis pipeline would improve the current statistics on the total number of detected microlensing events. The construction of such tools in the framework of IDA will substantially increase the possibilities for Danish astrophysics to benefit optimally from the very start from huge investments that are planned internationally in the coming years into extreme large sky survey and monitoring programs.

This report represents an overview of current and future survey projects and outlines the basic idea in the development and integration of software tools (using existing image analysis algorithms and software) for the on-line retrieval, acquisition and processing of single field photometric data obtained from sky survey projects. Software integration into a single automated data retrieval and processing pipeline, will encompass an early alert warning system for upcoming gravitational microlensing events. In a final implementation, a software based microlensing early alert warning system will have application within the context of the Danish initiated SONG project suitable for conducting follow-up observations of gravitational microlensing events. A review of existing and currently on-going early alert warning systems is presented and the basic theory for understanding gravitational microlensing is outlined.

Chapter 2

The gravitational microlensing technique

2.1 Introduction

According to Einsteins general theory of relativity one of the fundamental large-scale principle in nature is as follows: *massive objects dictate space-time how to curve; and curved space-time dictates light how to propagate within a material universe.* As a natural consequence, massive objects will have a deflecting effect on nearby travelling light rays. The deflection angle is given by

$$\alpha = \frac{2R_S}{u}, \tag{2.1}$$

where $R_S = \frac{2GM}{c^2}$ is the Schwarzschild radius of the lens and u is the impact parameter, measuring the distance of closest approach of the light ray to the massive lensing object of mass M (cf. Fig. 2.1).

Light rays from a distant source are focused by an intervening massive object resulting in both a change in the apparent position of the source on the sky and its brightness. In a first order approximation, the source is split into two images. If a change in the position of the images is observed the phenomenon is resolved and known as the *gravitational lensing effect.* The lensing ability of material objects has been proposed by Einstein and independently by Link in 1936 (Perryman, 2000, p.31). The effect of gravitational lensing is identified by the appearance of separated luminous arc or point-like images around an (unseen) lensing object. The lens itself is often represented by a massive nearby galaxy or a cluster of galaxies and the luminous arc-like images can be associated to a single light source represented by a distant background galaxy (Lynds and Petrosian, 1989).

If the masses involved are small and distances are of order galactic distance, the effect of image separation by gravitational lensing can no longer be resolved. How-

ever, the effect of gravitational lensing manifests itself by a unique variation in observed object brightness. This case is known as *gravitational microlensing*. The term microlensing is introduced from the fact that images are separated on the order of micro-arcseconds for a solar mass lens at cosmological distances. If lensing stars are positioned within Galactic distances the separation is of order milli-arcseconds[1].

Several astrophysical applications for gravitational microlensing exist: Paczyński (1986a) stressed the possibility to apply the microlensing technique as an observational tool to probe the distribution of compact dark matter objects within the galactic halo. Later Mao and Paczyński (1991) and Gould and Loeb (1992) proposed and outlined the search for galactic binary stars and planets in extrasolar planetary system by observing star fields towards the galactic bulge. Since then several monitoring programs were initiated with a massive search for stellar variability. The existence of microlensing events were demonstrated by observations in the beginning of the 1990s. For a review see Paczyński (1996).

2.2 Theory: magnification, scales and binary lensing

Microlensing geometry

Microlensing involves three components (cf. Fig. 2.1): the observer (O), a massive star (lens object, L) and a background field star (source object, S). In a first approximation of the theory, objects are assumed to be point masses and we denote this simplification as the *point source, point-mass lens (PSPL) model*. Figure 2.1 represents the basic observer-PSPL geometry.
In the case of the absence of a light deflecting object, the source is observed under the angle β. In the case of an intervening massive lensing object, the apparent angular position of the source object at S_1 is observed under the angle $\theta = \alpha + \beta$. The actual position $\beta = \beta(t)$ of the source is a function of time. Within the PSPL model approximation the geometry of lensing (i.e the positions θ, where images will be observed after light is deflected by a massive lens object) is expressed by the *lens equation* (Paczyński, 1986a)

$$\theta^2 - \beta\theta - \alpha_0^2 = 0, \tag{2.2}$$

where $\alpha_0^2 = \frac{2R_S D_{LS}}{D_L D_S}$. Two solutions (θ_1, θ_2) to this quadratic equation in θ exists and represents the angular position of two images. This is shown in the right panel of Fig. 2.2 and denoted by (I_1, I_2). In the dynamical case the images are changing

[1]However, Paczyński (1986a) introduced the notion of adding unresolved micro-images resulting in a single observable macro-image changing in brightness

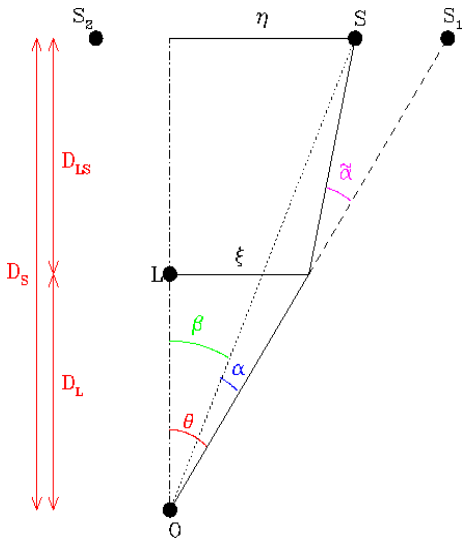

Figure 2.1: Snapshot of the basic geometry of a microlensing event. O : Observer, S : source object and L : massive lens object. The angular position $\beta = \beta(t)$, is a continouse function in time. Due to the lensing effect of L, the fictouse source (S_1) is observed under the apparent angle θ. For the impact parameter ξ a light ray emanating from S is deflected by the angle α.

position according to the transversal motion of the source object relative to the lens (the motion is from left to right in the right panel of Fig. 2.2. The source is indicated by a blue circle).

In the case ($\beta = 0$) of a perfect alignment between the observer, the lens and the source, both images will join and form a luminous ring-like image (denoted as the Einstein ring). For a typical galactic microlensing case ($D_L = 4$ kpc and $D_S = 8.5$ kpc) the order of magnitude for the diameter of the Einstein ring is a milliarcsecond ($\approx 0.001''$). This angle is too small in order to be resolved with any existing telescope.

Magnification and the light curve

The time variation of the apparent brightness of the source is proportional to the variation of the combined magnification of the two images. The time of maximum magnification is represented by the time of closest approach between the source and the lens. The total magnification is a function of time and given by (Paczyński, 1986b, 1996)

$$A(u) = A_1 + A_2 = \frac{u^2+2}{u(u^2+4)^{1/2}}, \quad \text{with} \quad u(t) = \left(u_{min}^2 + (2(t-t_0)/\hat{t})^2\right)^{1/2}, \quad (2.3)$$

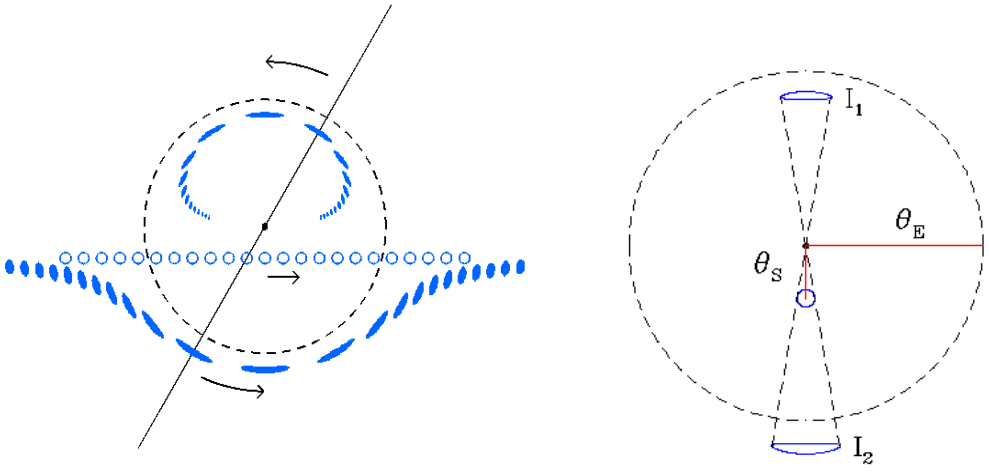

Figure 2.2: Left panel: Within the PSPL model one image (I_1) is located within and the other (I_2) is located outside the Einstein ring. The outer image is always brighter compared to the inner image. The motion of the source object is from left to right. Right panel: Image position at closes approach between the source and the lens. In the figure, $\theta_S = \beta$ denotes the angular position of the source and the lens is located in the image centre. θ_E is the apparent angular extend of the Einstein ring. The Figures are reproduced from P. Sackett (http://www.mso.anu.edu.au/∼psackett/NVWS/Microlenses.html)

where $u(t) = \beta(t)/\theta_E$ is the impact parameter, t_0 is the time of peak amplification and $\hat{t}$ is the duration of the microlensing event (i.e defined by crossing the Einstein ring). u_{min} is the impact parameter at peak amplification $A = A_0$. Thus the signature for a microlensing event is a time-symmetric brightening of a star occurring as a massive object passes close to the line-of-sight. The simplest form of a microlensing lightcurve is then uniquely determined by the model parameters $(A_0, t_0, \hat{t})$. Physical information about the lensing object is contained in $(\hat{t}, \theta_E)$, from which the lensing objects Einstein ring crossing time, relative velocity and mass is determined. The brightness change of the background source star depends on the angular separation of the source and the lens at closest approach. If the angular position of the source at closest approach is $\beta = \theta_E$ (corresponding to the Einstein ring) the total magnification is $A \simeq 1.34$. The brightness varies more for passages with a smaller impact parameter. For angular separation smaller/larger than θ_E the magnification is greater/smaller than 1.34. Microlensing events outside the lensing zone can be observed, if a brightness variation smaller than a factor 1.34 (in magnitude) can be detected.

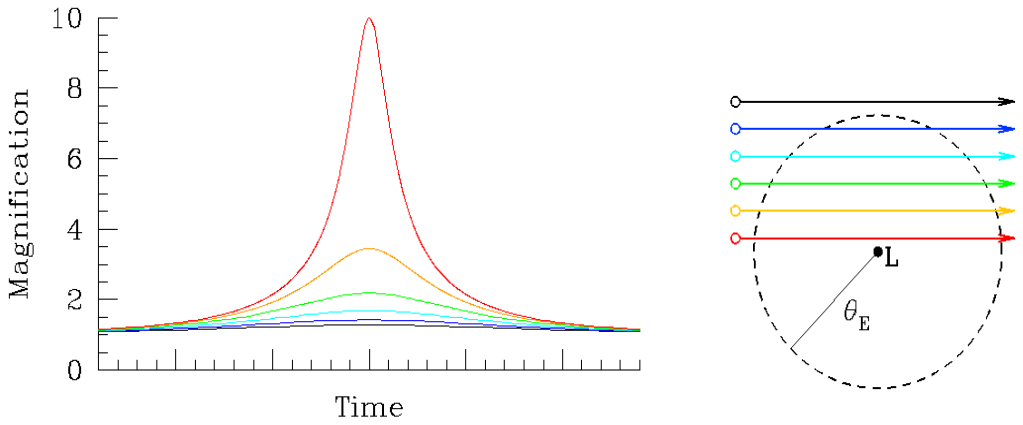

Figure 2.3: Magnification of a background source star as a function of the angular separation (or impact parameter) between the lens and source object. The various projected paths of the source are colour coded and the lens object is located at the centre of the right panel figure. Note that the apparent path of the source object could be any given random oriented trajectory within or outside the Einstein ring radius. Because of the non-clumping nature of stars observed towards the galactic bulge the probability of a smaller/larger magnification is larger/smaller. The Figures are reproduced from P. Sackett (http://www.mso.anu.edu.au/∼psackett/NVWS/Microlenses.html)

Microlensing time scales and event frequency

The form of the light curve depends on the particular geometry for a given microlensing event. For practical reasons the following quantities are introduced. Assuming $D_S \gg D_L$ the linear Einstein ring radius is (Paczyński, 1986b)

$$R_E \simeq \theta_E \times D_L \simeq 1.4 \times 10^{14}\text{cm} \left(\frac{M}{M_\odot}\right)^{1/2} \left(\frac{D_L}{10 \text{ kpc}}\right)^{1/2}, \tag{2.4}$$

The expected time scale for the brightness variation during a microlensing event is obtained from the tangential velocity of the source and the radius of the Einstein ring. For a lensing object at distance $D_L = 4$ kpc moving with a velocity $v \simeq 220$ kms^{-1} the Einstein ring crossing time is given by

$$t_E \equiv \frac{R_E}{v} \simeq 3.8 \times 10^6\text{s} \left(\frac{M}{M_\odot}\right)^{1/2} \simeq 44 \text{ days} \left(\frac{M}{M_\odot}\right)^{1/2} \tag{2.5}$$

For a solar mass lensing object the typical time scale for a microlensing event (assuming $D_S \gg D_L$) is on the order of 5 weeks. The time of maximum magnification is, when half the Einstein ring is traversed. However, the probability of observing a perfect aligned microlensing event is rather small and the above estimation represents an upper bound for the event duration.

The frequency of microlensing events is estimated using the total number of lens stars contained within a given cone of length D_S with angular aperture corresponding to the angular extend traversed by the moving source object. All lensing objects have angular extend equal to their angular Einstein ring and have equal mass. From this consideration lens objects located closer to the observer contribute with a larger probability of microlensing alignment. The average time interval between microlensing events is then given by (Paczyński, 1986b)

$$\langle \Delta t \rangle \simeq \frac{t_E \pi R_E}{2N\tau\xi} \simeq \frac{1.5 \times 10^6}{N} t_E, \tag{2.6}$$

where N is the total number of stars monitored, τ is the probability that the source is found within R_E and ξ is the impact parameter with $\xi/R_E < 1$. Adopting $t_E = 44$ days and $N = 10^6$, we should expect a single event within 66 days or 6 events in a year. This number is clearly to small for practical applications and the total number of stars within a monitoring survey program should be within $10^7 < N < 10^9$, corresponding to average time intervals between two consecutive microlensing events of 4 minutes to 7 days.

Binary lensing and caustic crossing amplification

In the general case for which the lensing object is not well described by a point like (e.g cluster of galaxies acting as a lens) object, several images at different angular positions are observed. Within the framework of gravitational microlensing a possible deviation from the point-mass lens, point source approximation is represented in the case of a binary star acting as a lens. If the components within a binary star are well separated (on the order of several Einstein radii) then each star can be considered as individual point-mass lenses.
A different behaviour in the light curve is observed for close binary components acting as a lens. In this case additional strong lensing effects (due to the combined gravitational fields of each component) are possible and observed as *anomalies* deviating from the time-symmetric PSPL light curve.

The region of additional amplification is called the *caustic region*. Positions of corresponding images are called *critical curves*. In the case of a single lens perfectly aligned with the observer and the source the caustic region is a single point behind the (unseen) lens and the critical curve is the Einstein ring (Griest and Safizadeh, 1998). Strong amplification(s) occur at positions located within the caustic region. Physically, the mathematical caustic curve is the region in which multiple light rays collect and additional images contributing to the total brightness are created. The passage of a caustic region is not always guaranteed and depends on the geometry of a given microlensing event.

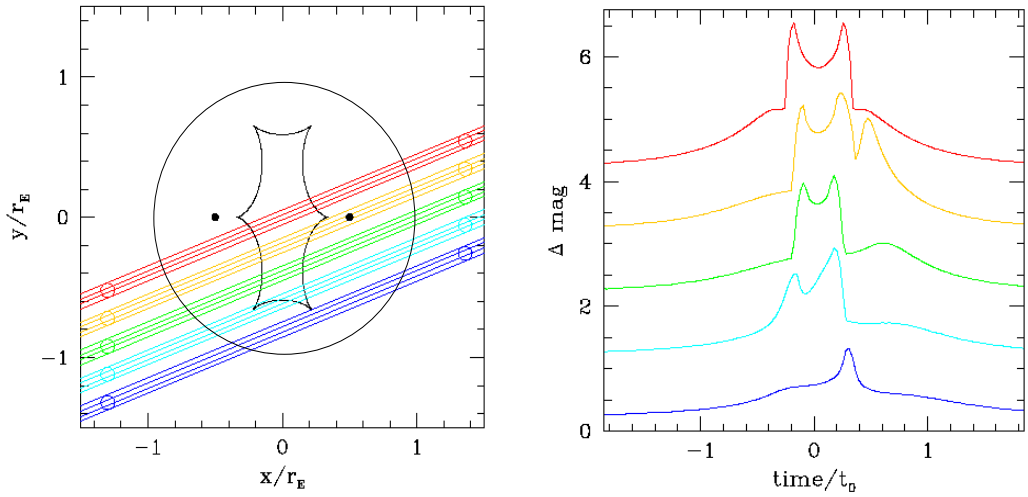

Figure 2.4: The geometry of microlensing events as projected onto the sky and their corresponding light curves. Left panel: several scenarios for the passage of a source star behind a lensing binary star are shown and colour coded for 5 different paths. Right panel: the corresponding light curve for each geometry is shown. The brightness is expressed in magnitude difference and increases upwards. The magnitude is related to the magnification by $\Delta m(t) = 2.5 \log(A(t))$. The figures are reproduced from P. Sackett (http://www.mso.anu.edu.au/∼psackett/NVWS/Microlenses.html)

In the case that the source star is passing through a caustic region, sharp amplifying peaks within the light curve mark the entry and exit points of the caustic region. Several scenarios for a caustic passage are possible. Figure 2.4 demonstrates the possible outcome for different caustic passages considering a binary star lens. The corresponding light curves are shown for each passage of the background source star. The black dots represents the position of the binary components on the sky and angular distance is measured in units of Einstein angular radii. From the figure the caustic region is characterised by several cusps and the exact form is determined from the components mass ratio. The lowest amplification is introduced when the projected passage is a near-cusp encounter (blue). The largest amplification is introduced when the passage traverses the caustic region and is characterised by two peak amplifications corresponding to the entry and exit points on the caustic curve. Additional forms of anomalous light curves are shown for intermediate caustic crossings. In all cases within the figure, a caustic (or near-caustic crossing) is associated with a peak in the observed light curve. However, the possibility of de-magnification also exist and is observed by local minimum within the light curve. This corresponds to the annihilation of unresolved magnified images during the caustic passage. It is important to note that the passage of a caustic (or near-caustic) region is needed in order to observe the existence of binary star.

2.3 Planetary microlensing observations and requirements

The more interesting case is given when one of the binary components is replaced by a planet companion acting as an additional sub-lens. Considering this situation Mao and Paczyński (1991) demonstrated the effect of strong amplification of *planetary caustic crossings* and suggested to use microlensing for future planet search programs. Depending on the mass ratio in the star-planet lensing system, several distinct caustic regions can emerge. The area size of caustic regions is proportional to the planet detection probability. The requirement to detect light curve anomalies attributable to planetary mass objects, is the crossing (or near-crossing) of the caustic region. Only microlensing geometries in which the source star trajectory is passing (near or through) the caustic region reveals the presence of a planet. All other configuration involving a planet will remain undetected.

Figure 2.5 artificially demonstrates the gravitational effect of Earth-mass planets on an observed high-magnification light curve. The lensing system considered con-

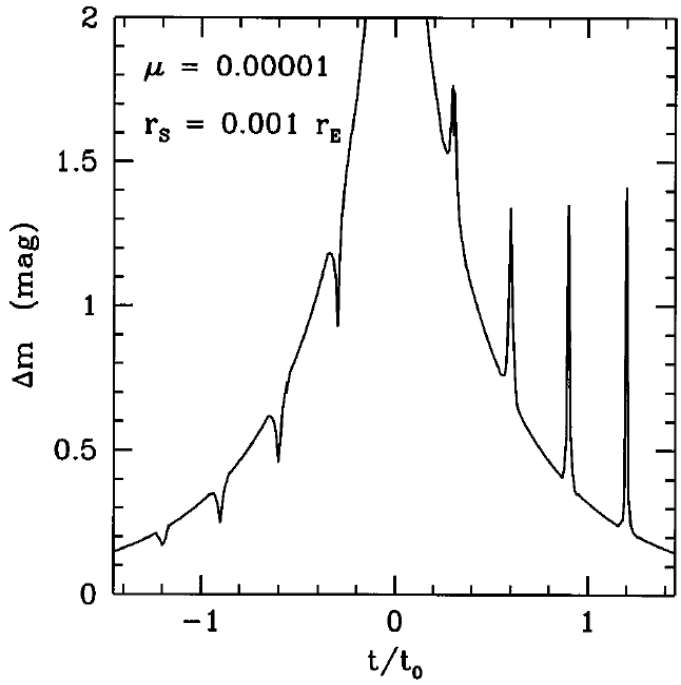

Figure 2.5: Modelling the lensing effect of eight Earth-mass planets within an artificial scenario in which the source trajectory is coinciding with the line of aligned planets. The mass ratio is denoted by μ and the source star is separated from the lens star by $10^{-3}\theta_E$ indicating a very high-magnification event. The Figure is taken and reproduced from (Paczyński, 1996).

sists of eight Earth-mass planets and the source object trajectory coincides with the line of aligned planets. Four planets induces de-magnification anomalies within the light curve, shown by small minimum. Each planet has a mass ratio of $m/M = 10^{-5}$. By considering the caustic area crossing time Mao and Paczyński (1991) estimated the duration of a typical anomaly (the duration of a single spike within Fig. 2.5) to be $\Delta t_{planet} \simeq 2.5 - 10$ hours for Earth to Jupiter mass planets. This short period addresses the question of sampling frequency for observations within follow-up observation programs. If the sampling frequency is too long, short duration anomalies within microlensing events are likely to be missed.

The detection and observation of extrasolar planets using the microlensing technique have been announced recently (Bond et al., 2004; Udalski et al., 2005; Beaulieu et al., 2006; Gould et al., 2006). All four reports presents observations consistent with a binary microlensing model adopting a small mass ratio. The microlensing events were triggered by the OGLE/MOA early warning monitoring systems. Subsequent follow-up observations were conducted by both the PLANET, RoboNet, μFun and OGLE/MOA collaboration programs.

The observed light curves are shown in Fig. 2.6. In the right panel figure the light curve anomaly is reproduced from a theoretical binary model and corresponds to a 1.5 Jupiter-mass planet with orbital radius ~ 3 AU (Bond et al., 2004). For this event the source crosses the Einstein ring in ~ 61 days. Two spikes on the left rising wing of the light curve indicate the entry and exit times of the caustic region and corresponds to caustic amplifications attributable to a Jupiter planet. The duration time of the caustic crossing spans ~ 7 days.
The left panel in Fig. 2.6 shows a light curve anomaly corresponding to a 5.5 Earth-mass planet. Observations were mainly obtained within the PLANET collaboration using a network of telescopes on the southern hemisphere (Beaulieu et al., 2006), but included also datapoints from OGLE and MOA. The Einstein ring crossing time (equivalent to the total event timescale) corresponds to ~ 25 days. The short-duration low-amplitude planetary amplification on the declining (right side) PSPL light curve corresponds to ~ 15 hours. In this event the lens star is a 0.22 $M_{\odot}$ star located at a distance of 7 kpc towards the galactic bulge.

Planet detection probability, high magnification events and the lensing zone

To increase the probability of detecting a possible lensing planet the random trajectory of the source star needs to pass nearby or through a caustic region in order to introduce significant perturbations on the lensing light curve. For a microlensing event with a lensing planet, two sets of caustic regions are produced. The first is displaced away (*planetary caustic*) and the other is located close (*central caustic*) to the primary lens star. The form and size of the caustic structures depends on the planet-lens mass ratio $q = m_p/m_l$ and projected distance r (Griest and Safizadeh, 1998; Chung et al., 2005).

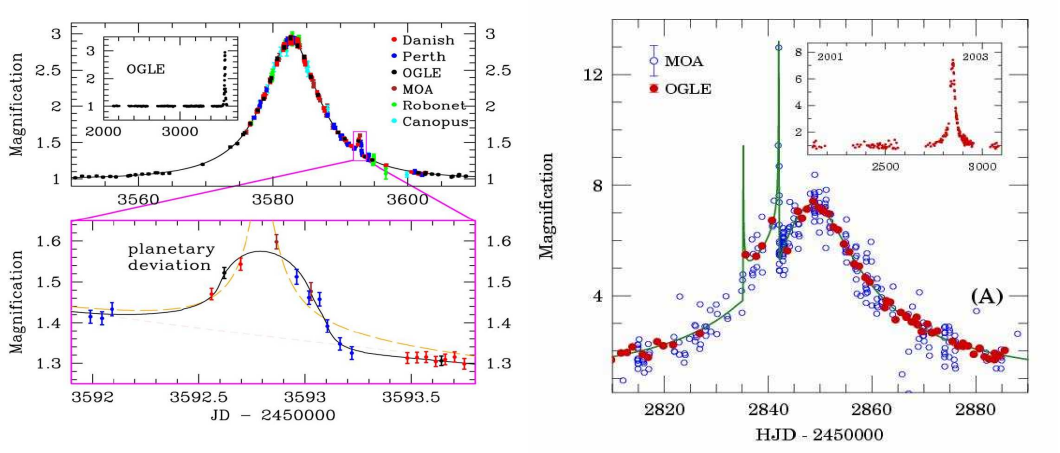

Figure 2.6: Observed microlensing light curves with light curve anomalies indicating the presence of extrasolar planets. Left panel: Light curve observations obtained within the PLANET collaboration and indicating the presence of a 5.5 Earth-mass planet at 2.6 AU (Beaulieu et al., 2006). Right panel: Observed light curve with deviations indicating a Jupiter-mass planet at 3.3 AU (Bond et al., 2004). The onset of both microlensing events were triggered by the OGLE early warning survey system and previous monitoring observations are shown in the respective inlet figures.

For a wide range of mass ratios and projected distances the form and size of the caustic structures can be complicated.

In the absence of a lensing planet the central caustic region is symmetric and located around the lensing star. In this case and to a first order approximation a close encounter (i.e high-magnification event) between lens and source star would result in a smooth symmetric PSPL lensing light curve.

The probability of detecting planets depends on the size of the *outer* planetary caustic region: the larger the caustic size the higher the probability to cross this region for a random projected source star trajectory. Gould and Loeb (1992) evaluated the probability of detecting a Jupiter-mass planet in orbit around a solar like lens star. Maximising the planet detection probability requires the projected planet position to be within $0.8 < r/R_E < 1.7$ from the lens star. This range is known as the *lensing zone* and corresponds to a physical distance of the planet within 1 - 10 AU. Considering this range and requiring a 2 - 5 % caustic deviation in the light curve (~ 0.05 mag.), Gould and Loeb calculates a 20 % probability to detect a Jupiter-mass planetary signal. Considering the detection probability of Earth-mass planets Bennett and Rhie (1996) calculates a 2 % chance to detect all Earth-mass planets within the lensing zone.

More importantly, a *central* caustic crossing of the source star improves the overall planet detection efficiency and the special case of a high-magnification event provides an enhanced sensitivity for planet detection (Abe et al., 2004). Again, the form and size of the central caustic structure depends on the planet-lens mass ratio and the

mutual projected lens-planet distance. This observational advantage was first pointed out by Griest and Safizadeh (1998) (and references therein) showing a 100 % detection probability of Jupiter-mass planets, if such a planet is located within or near the lensing zone (i.e 1 - 10 AU from the central host star).

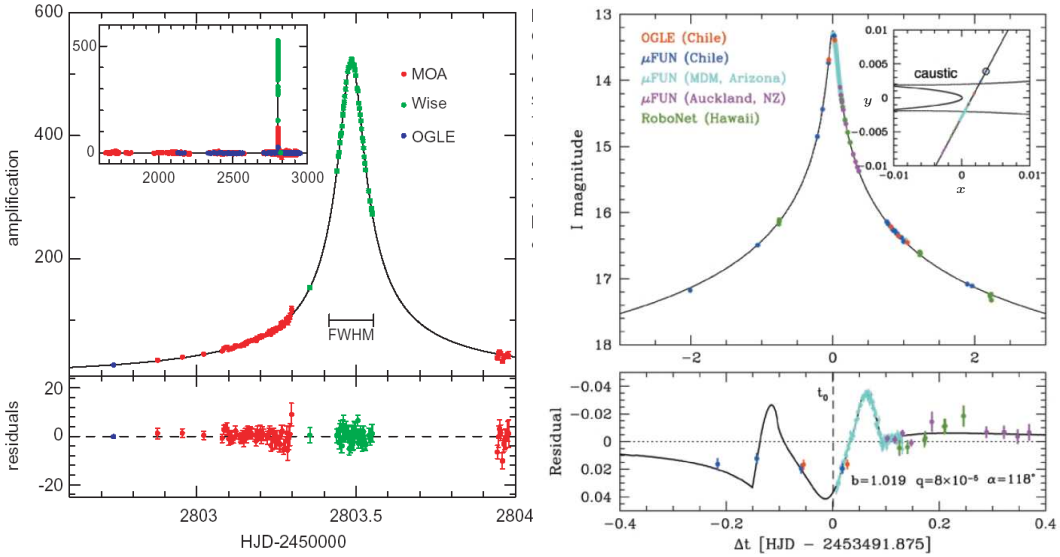

Figure 2.7: Examples and comparison of two high-magnification events. *Left panel*: Observations of the high-magnification lensing event MOA 2003-BLG-32/OGLE 2003-BLG-219 with peak magnification $A_0 \sim 500$. I-band measurements are well fitted by a theoretical PSPL light curve. A residual analysis did not show any deviations from the PSPL light curve possibly indicating the existence of a planet. The inlet figure shows OGLE/MOA monitoring measurements prior to the onset of the microlensing event. The FWHM crossing time is $\sim$ 2.4 hours and the Einstein ring crossing time is $t_E \sim$ 20 days. The figure is reproduced from (Abe et al., 2004). *Right panel*: A high-magnification event (Gould et al., 2006, μFUN collaboration) indicating the presence of a Neptune-mass planet ($q \sim 10^{-4}$, with $m_l \sim 0.5\ M_\odot$). The peak amplification is at $A_0 \sim 800$. The planet induced perturbation on the light curve reveals itself in the residuals which shows systematic deviations (3 - 4 %) from a non-planet PSPL model. The inlet figure reflects the projected trajectory of the source star through the central W-shaped caustic region. The lens star is placed at $(x, y) = (0, 0)$.

In the presence of a lensing planet the symmetric central caustic region is distorted and replaced by a W-shaped region (cf. right panel in Fig. 2.7). This caustic difference introduces an observable effect. For a random source star trajectory passing near the central caustic region (or lens star) this effect is translated to an observable deviation in the single-lens PSPL light curve. For different high-magnification scenarios Griest and Safizadeh (1998) showed that if the peak amplification is monitored densely and the lens star is orbited by a planet, events with a maximum amplification of $A_0 \sim 50$ would reveal a Neptune-mass planet. If a terrestrial low-mass planet has an orbital radius around one Einstein radius corresponding to a few AU, a central asymmetric

caustic structure will always be present near the lensing star.

Further simulations of planetary microlensing during high magnification events considered the detection probability of Earth-mass planets for observations sampled over the FWHM of the light curve (Rattenbury et al., 2002). They showed that Earth-mass planets are detectable, if their projected orbital radii are within 1.5 - 2.5 AU. In addition, Rattenbury et al. confirmed that giant planets are detectable within 10 AU.

The unsuccessful detection of a planetary signal during a high-magnification event can be used to eliminate the possible presence of terrestrial and giant planets over large orbital radii (Bond et al., 2002). Observing several high-magnification events could place fairly strict upper bounds on the abundance of these planets. Abe et al. (2004) and Dong et al. (2006) demonstrated the absence of any planetary signal during a high-magnification event and excluded the existence of lensing planets over a large range of orbital radii. The left panel in Fig. 2.7 shows a high-magnification light curve in the absence of a planetary signal.

By observing many high-magnification microlensing events in high time resolution, one will eventually be able to combine the statistics from the detections and non-detections into a picture of the statistics of various mass planets in various orbits around the full population of stars in our Galaxy. This analysis, hence, include the answer to the question of how many habitable planets exist within the Milky Way galaxy.

2.4 Microlensing advantages and challenges

Advantages

- Microlensing observation and detection is complementary to other planet search techniques (like radial velocity technique).

- Instantaneous snapshot of the system. No need for long-duration monitoring surveys to wait for planets at large orbital distances to complete a single orbital period.

- After the detection of an anomaly the characterisation of the planet can be achieved during a few hours or days.

- Microlensing is more sensitive to smaller-mass planets than most other techniques and is the only method substantially sensitive to Earth-mass planets with orbital radii within 1 - 10 AU.

- For high magnification events more flux is available which increases the signal-to-noise ratio and reduces the photometric Poisson error (photon noise). This

implies that high accuracy photometry will generally be available during the peak amplification period.

- High magnification events have a higher probability in detecting Neptune to Jupiter-mass planets and only the FWHM time span needs to be sampled densely for a proper characterisation.

- Easy to distinguish from other periodic variable objects, since microlensing events should never (statistically) repeat for the same target star.

Challenges to consider

- Galactic microlensing events cannot be predicted in advance. Therefore, it is necessary to observe and monitor $10^7 - 10^8$ stars towards the Galactic bulge (and/or within the Galactic plane) within a microlensing alert survey program.

- Microlensing is not appropriate for detailed studies of individual nearby planetary systems. It only provides statistical data on the mass ratio, orbital separation and the frequency of planets.

- One-time event only. No opportunity for repeating measurements: a detectable microlensing signal will occur one time per planetary system. The probability of a microlensing event at any given time is 10^{-6}. The probability that a given event will reoccur at a later time is even smaller.

- Continuous sampling of a given microlensing event requires a ground-based, longitude-distributed network of automated telescopes.

Chapter 3

Microlensing survey and follow-up programs

3.1 Introduction

The fundamental idea of Galactic microlensing surveys is to search for stellar brightness variation and magnification in a large number of observed stars. Because of the infrequent occurrence of microlensing events, it is necessary to observe high stellar density fields within a continuous monitoring survey. Several targets have been of interest within different survey programs: the Large Magellanic Cloud (LMC), the Galactic Bulge (GB) and the Small Magellanic Cloud (SMC).

The use of Galactic microlensing as a tool to probe the matter distribution and structure of the Milky Way was first proposed by Paczyński (1986a,b), in order to detect dark halo objects by monitoring millions of stars towards the Magellanic Clouds. Shortly afterwards, Mao and Paczyński (1991) recognises the important application of Galactic microlensing as a tool for planet detection and today the majority of microlensed planetary systems are observed and detected towards the Galactic bulge.

Many objects exhibit brightness variations on different time scales and the nature of object variability is not always clear. Sophisticated photometric analysis is necessary in order to distinguish between different types of variations. Modern implementations of photometric data reduction pipelines allows the detection and warning of an interesting microlensing candidate in nearly real-time. Early detections of microlensing events can be important for dense sampling or follow-up observations.

Since early and mid-90s, several collaboration groups have formed to perform microlensing observations within monitoring surveys or follow-up campaigns: EROS, OGLE, SuperMACHO, MOA, PLANET and μFUN. For a review of initial microlensing search campaigns, first results and future development see Roulet and Mollerach (1997) and Mao (2001)). At current time the most effective microlensing monitoring

and survey programs are the OGLE and MOA observing campaigns. Follow-up observations of individual microlensing events are performed mainly by PLANET, RoboNet and μFUN. In the following, a review of these survey and follow-up programs is presented.

3.2 OGLE

The OGLE (Optical Gravitational Lensing Experiment) is a collaboration between Warsaw University Observatory, Carnegie Observatory and Princeton University Observatory (http://bulge.princeton.edu/∼ogle/). The OGLE project primary task is the continuous monitoring of star fields toward the LMC, SMC and the GB to search for microlensing phenomena. Since the beginning of the OGLE project three subsequent upgrade phases were considered involving major improvements in hardware components and telescope equipment.

	Target(s)	Events	Time	Instrument	FOV	Colors
OGLE-I	Bulge	20	92-95	$2k \times 2k$, 1.0m	$15' \times 15'$	I (+V)
OGLE-II	Bulge	150	97-00	$2k \times 2k$, 1.3m	$15' \times 15'$	I (+V)
	LMC	1				
	SMC	0				
OGLE-III	Bulge	~ 2635	01-06	$8k \times 8k$, 1.3m	$35' \times 35'$	I (+V)
	LMC	0				
	SMC	1	01-06			

Table 3.1: Overview of OGLE survey and instrument data. Note the low event rate towards the LMC and SMC from the beginning of OGLE-II phase. The OGLE-III (2001) monitoring campaign adopted a larger field-of-view (FOV) thereby increasing the detection rate of microlensing events. The table is reproduced from Mao (2001) and complemented with recent OGLE-III survey data and instruments specifications taken from the OGLE project homepage.

The first observing campaign (OGLE-I) started in 1992 using the Swope 1m telescope at the Las Campanas Observatory (Chile), operated by the Carnegie Institution of Washington. The first generation CCD camera used a 2048×2048 CCD detector with individual 24μm pixels resulting in a $0.42''$/pixel scale. This corresponds to a $15' \times 15'$ field of view on the sky. From 1997 regular observations were carried out within the OGLE-II project phase using the new 1.3m Polish Telescope (Warsaw University). Table 3.1 gives an overview of OGLE project survey and instrument data. Hardware improvements within the OGLE-III survey phase, by installing a large-array CCD camera at the cost of a lower S/N ratio, increased the sky area coverage by a

factor of 5. As a consequence the seasonal average microlensing detection rate towards the Galactic bulge increased by a factor of 10 from $\sim$ 50 (1997 - 2000, OGLE-II) to $\sim$ 520 events (2001 - 2006, OGLE-III). During the OGLE-I survey and monitoring phase a total of 20 microlensing events were recorded during the observing seasons 1992 - 1995.

OGLE-III

In 2001, the most recent hardware upgrade for the OGLE-III data acquisition system were introduced (Udalski, 2003). A large-field CCD mosaic camera (composed of eight $2k \times 4k$ CCD chips) with a $0.26''$ CCD pixel scale were installed, corresponding to a total field of view of $35' \times 35'$ on the sky. Fig. 3.1 shows the current OGLE-III survey fields towards the Galactic bulge.

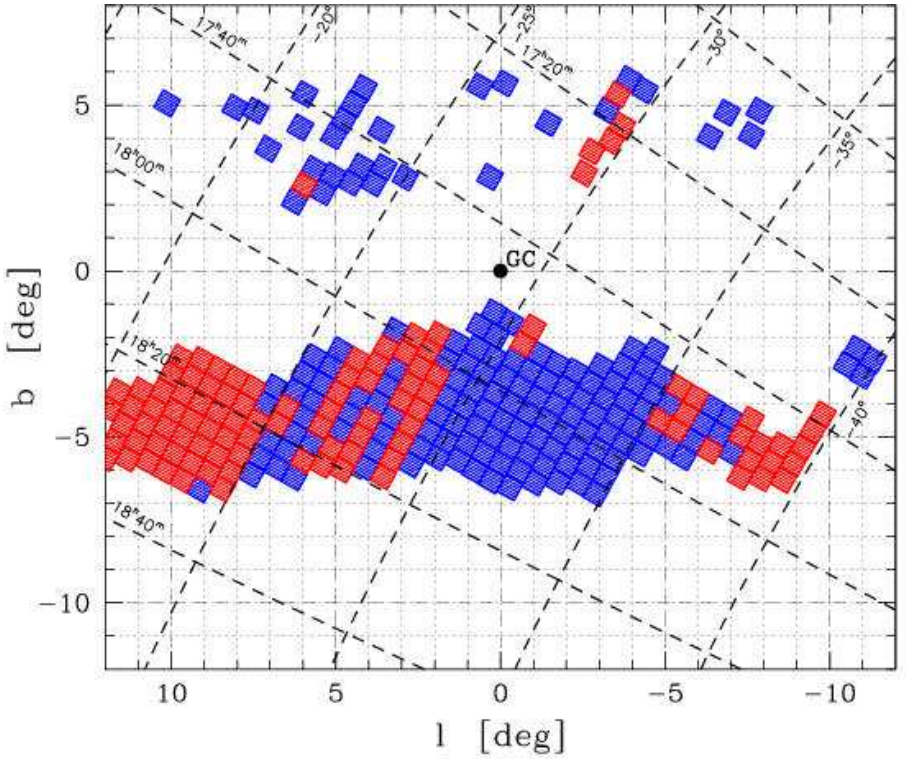

Figure 3.1: Survey target fields toward the Galactic Bulge within the OGLE-III monitoring campaign. The figure provides equatorial ($RA, Dec.$) and galactic coordinates (l, b). Each field corresponds to $0.58° \times 0.58°$ on the sky. A total of 37 fields are observed for $b > 0°$ and 238 fields for $b < 0°$. The total observed area corresponds to $\sim$ 92 deg.^{2}. Blue colored fields are priority fields monitored frequently. The centre of Baades Window is located at $(l, b) = (1°, -3.9°)$.

A total of 200 million stars are frequently monitored (170 million stars towards the

GB and 30 million stars towards the Magellanic clouds). The majority of frames are observed in the photometric I-band. During a given season the median seeing is $1.3''$ and the observed photometric magnitude error is 2-10% for faint stars near $I = 18 - 20$ mag.

For a CCD readout time of ~ 100 seconds and assuming an average exposure time of ~ 200 seconds each field is sampled once for every ~ 23 hours (or once every night). However, the typical sampling of Galactic bulge fields during the 2002-2003 observing season was on average one field every 1.5-2 nights. Low priority fields (those with low number of detected microlensing events) are sampled once every 2-4 nights.

Regular monitoring of OGLE-III fields is performed during the winter season on the Southern Hemisphere. The equatorial latitude of the Galactic bulge centre is near $\delta = -30^{\circ}$ latitude. Regular observing season spans from early April to mid September. Reduced photometry data of microlensing events are released in nearly real time within a given observing season and light curve data are available to public domain on *www* or *anonymous ftp*.

The OGLE-III data reduction and image analysis pipeline is fully automated and divided into three main steps: 1) raw image reduction by flat fielding and bias subtraction, 2) CCD image alignment and difference image analysis (DIA) (Alard, 2000) and 3) aperture and profile photometry on the difference image. The difference image analysis technique is specially designed for accurate photometry of crowded/blended CCD star field images. Difference imaging enables microlensing events to be detected with faint source stars (usually dwarf stars) that are undetectable when unmagnified. This has the advantage of increasing the number of detection events by 85% compared to standard differential PSF photometry (Alcock et al., 2000). For each star field a photometry database is created holding an identification number of each object, observed object $I-$band magnitude and the corresponding magnitude 1σ-error.

OGLE-III microlensing detection system

Detection of microlensing events requires an automated warning system informing on the brightness change of a given object. The detection of a microlensing event is controlled by the OGLE-III early warning system (Udalski, 1994, 2003). Within the currently ongoing Galactic bulge monitoring survey a total of 170 million non-variable stars are identified and registered within a database. The system was designed to detect any kind of transient or stellar variability in real time. Several criteria needs to be passed for the detection of a true microlensing event.

After each observing night photometric measurements for each object are derived and the database is updated. The new measurements are then compared to the seasonal mean magnitude for each object within the non-variable object database. In order to detect brightness variability the system checks for an increase in brightness according to a brightness threshold. If 4 subsequent measurements of an objects brightness exceeds

a predefined limiting magnitude, then the object is flagged as a potential candidate of an ongoing microlensing event. The limiting magnitude is set to three times the average photometric error (3σ) within the data set.

Fig. 3.2 shows the detection of the first microlensing event (OGLE#11) during the initial OGLE-I survey season. The source object was observed for 850 days during the years from 1992 to 1994 and identified as a non-variable object with baseline I-magnitude, $I_0 = 18^m.20 \pm 0^m.01$. The threshold magnitude for microlensing detection is $3\sigma = 0^m.21$ and the average photometric error of individual measurements is $\sigma \sim 7\%$.

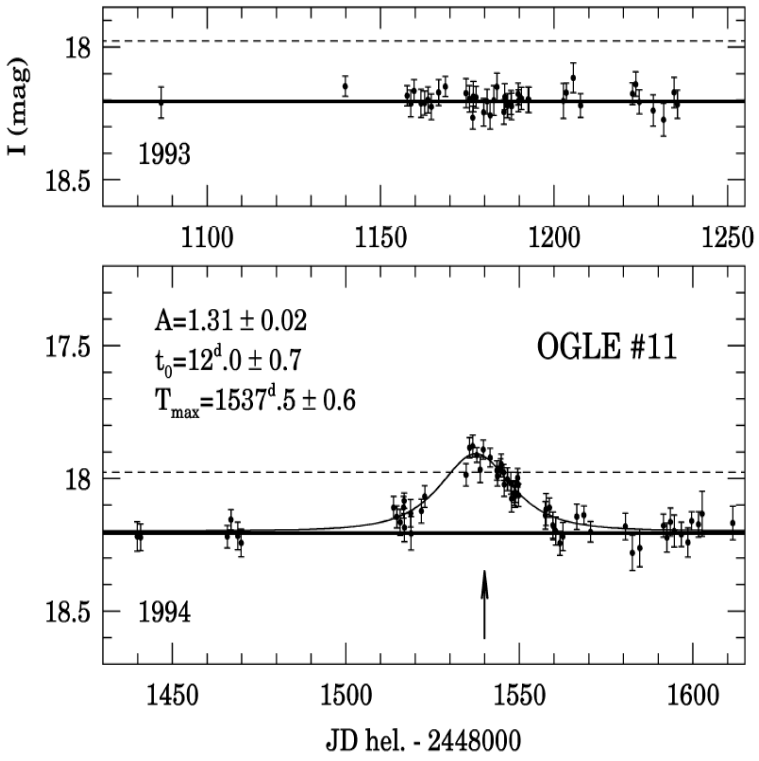

Figure 3.2: First detected microlensing event within the OGLE monitoring program (OGLE#11). The source star (non-variable) were monitored during a 2-years period. 5 consecutive measurements above the limiting threshold magnitude ($3\sigma \sim 0.21$ mag.) triggered the OGLE-I early warning system for a microlensing candidate. In this case the projected path of the source star was nearly tangent to the Einstein ring. Adopting a simple PSPL model for this event the light curve parameters are shown in the lower panel. The arrow indicates the 5th measurement above the 3σ level triggering an early warning of this microlensing event. After the detection the event were followed by a series of dense measurements further constraining the form of the event light curve. The scatter is mainly due to photon noise. The figure is reproduced from Udalski (1994).

3.3 MOA

The MOA (Microlensing Observations in Astrophysics[1]) project is a collaboration between Nagoya University, Japan and Universities of Auckland, Canterbury and Victoria and Carter Observatory, New Zealand using the Mt. John University Observatory in New Zealand. MOA is in operation since 1996 and was founded in 1995 undertaking both sky survey and microlensing follow-up observations. The primary task is a continuous monitoring of crowded star fields (unobscured by dust) towards the GB and the Magellanic Clouds. Real-time detections of microlensing candidates are announced on the MOA alert page[2].

During the first (MOA-I) phase of the project a 0.6m Cassegrain telescope was used with a 3-chip ($2k \times 4k$) mosaic CCD camera covering a 0.3 deg^2 field of view on the sky ($0.53^\circ \times 0.53^\circ$) (Bond et al., 2002). Highlights during the initial MOA-I observing seasons are (Hearnshaw et al., 2005, see references therein)

- Detection of the first confirmed extrasolar planet by microlensing.
- Detection and analysis of high magnification event MOA-2003-BLG-53.
- Measurements of the optical depth to microlensing towards the Galactic bulge.
- Contribution of photometric measurements of to the discovery of the second extrasolar planet by microlensing, OGLE-2005-BLG-71.
- Detection of 12 transiting objects with radii in the range $1.7 - 3.2 R_{Jup}$.

In 2004, the MOA project (MOA-II) was upgraded with a 1.8-meter mirror, wide field survey telescope, installed at the Mt. John Observatory (Hearnshaw et al., 2005). This telescope is fully dedicated for microlensing detections towards the Galactic bulge and LMC/SMC and routine observations in survey mode are commenced since the beginning of the 2006 GB season. The instrument uses a 10-chip ($2k \times 4k$) mosaic CCD camera. The CCD scale size is 0.57"/pixel corresponding to a total FoV of $1.32^\circ \times 1.65^\circ = 2.2$ square degrees on the sky. This large field allows millions of stars to be observed simultaneously. MOA typically takes 100s exposures for target fields towards the Galactic bulge and 300s towards the LMC/SMC (*private communication*, I.A.Bond). For these exposure times the limiting I-band magnitude for faint objects is around $I \sim 18$ magnitude.

[1] http://www.phys. canterbury.ac.nz/moa/

[2] http://www.phys.canterbury.ac.nz/moa/microlensing_alerts.html

3.4 PLANET

The PLANET/RoboNet (Probing Lensing Anomalies NETwork[3]) collaboration joins the observational effort of several 1m-class telescopes. The project is specialised for events on short time scales ($\sim$ 1 h) and the primary tasks are follow-up observations of alerted microlensing events.

The PLANET telescope network includes 6 telescopes located at different longitudes on the Southern Hemisphere. This configuration allow a nearly continuous monitoring of particular events. Within the collaboration the following telescopes are used

South America, Chile:

- The Danish 1.54m telescope at La Silla (ESO) observatory, Chile. CCD: 2048×4096 pixels (only a sub frame of 512×512 pixels is used for photometry). Pixel scale: 0.352 "/pixel. Corresponding to a $3' \times 3'$ field of view.

South Africa:

- The SAAO 1.0m telescope at Sutherland, South Africa. CCD: 512×512. Pixel scale: 0.35"/pixel corresponding to $3' \times 3'$ on the sky.
- The 1.52m Rockefeller telescope at Boyden Observatory, South Africa. CCD: 770×1152 pixels. Pixel scale: 0.206 "/pixel. FOV: $2.64' \times 3.95'$.

Australia:

- The 1.0m telescope at Canopus Observatory, University of Tasmania, Australia. CCD: 512×512 pixels. Pixel scale: 0.47 "/pixel corresponding to $4' \times 4'$ on the sky.
- The Perth 0.6m telescope at Bickley, Australia. CCD: 512×512 pixels. Pixel scale: 0.6 "/pixel corresponding to a $5' \times 5'$ field of view on the sky.

Additional telescopes:

- The Robonet telescope network. Three identical 2.0m-class telescopes. CCD: 2048×2048 pixels. Pixel scale: 0.135 "/pixel. Field of view: 4.6×4.6 arcmin.

[3]http://planet.iap.fr/ and http://www.astro.livjm.ac.uk/RoboNet/

3.5 MicroFUN

The Microlensing Follow-Up Network[4] is a collaboration of astronomers on 5 continents and based at Ohio State University, USA. The primary scientific objective is the follow-up observation of microlensing events with a preferential focusing on high-magnification events. Regular observations during the Galactic Bulge season are ongoing and in operation since 2003. Recently, the MicroFUN project (in collaboration with OGLE and Robonet) announced the detection of a Netptune-mass planet within a high-magnification microlensing event (Gould et al., 2006).

The network consists of several small- and medium sized telescopes ranging from 0.25m to 2.4m in mirror diameter. The following list is a selection of telescopes within the MicroFUN network.

- The 1.3m Cerro Tololo InterAmerican Observatory, Chile. CCD: 1024×1024 pixels. Pixel scale: 0.369"/pixel. FoV: $\sim 6' \times 6'$.
- The Farm Cove Observatory, Auckland, New Zealand using a commercial 0.25m Celestron Schmidt-Cassegrain telescope. CCD: 1024×1024.
- The 2.4m Hiltner telescope at the MDM observatory, Kitt Peak, Arizona, USA. CCD: 1024×1024. Pixel scale: 0.28 "/pixel. FoV: $4.78' \times 4.78'$.

[4] http://www-astronomy.mps.ohio-state.edu/∼microfun/

Chapter 4

Sky monitoring programs

4.1 Introduction

The onset of digital sky surveys have introduced a new standard in observational astrophysics. The scanning of the sky in different energy bands have revealed a new picture of the structure of the near and far universe. Existing optical all-sky surveys, however, only provide a *static* view of the night sky. Many interesting astronomical events occur on human and even daily time scales and represent the most difficult phenomena to observe. In order to capture recurrent and/or temporal short-term astronomical events, it is necessary to perform *continues sky monitoring* on a regular and frequent time basis.
A frequent mapping of the entire sky sets challenging demands on data handling, processing and storage. Nemiroff and Rafert (1999) provides a review of major (optical) sky survey projects and outlines a case study to realise a depth/brightness limited sky survey and monitoring system. Djorgovski et al. (2000) discusses some of these challenges and the application of sky survey data within Virtual Observatories (VO) and Mahabal et al. (2004) outlines a real-time transient phenomena detection data pipeline.

In the near future it becomes feasible to start a continuous digital record of the entire sky. An important prospect of intensive sky monitoring outcome, is the *real-time detection of microlensing events* (or, in general, the detection and identification of variable and transient sources). The detection frequency of microlensing events can be increased by using photometric observations obtained from recurrent sky survey programs. The primary survey and monitoring data product available to the end-user astronomer is a stellar object database enabling an opportunity for the search and analysis of transient/variable astronomical events.

Several survey telescope projects for rapid and recurrent sky mapping are currently under development (e.g. SkyMapper and VYSOS on the short-term, Pan-STARRS on

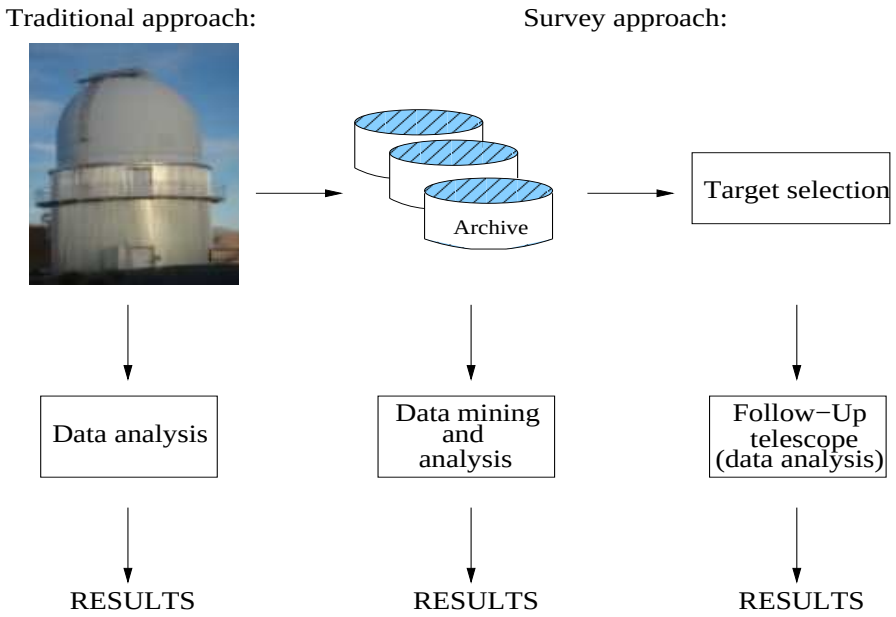

Figure 4.1: Traditional astronomical observation (left, vertical data flow, characterised by low data throughput) and data flow/processing of current astronomical survey programs like SDSS. Subsequent follow-up observations of specific targets are possibly supplemented with external data archives.

the intermediate and LSST on the long-term planning time scale). A useful measure of the survey power (SP) of a given telescope is proportional to the *étendue* (or the *telescope throughput* - the product of total collecting area and field of view) and is given by

$$SP \sim A\ \Omega, \tag{4.1}$$

where A is the collecting area of the telescope and Ω is the field of view (solid angle that is imaged on the CCD). Large surveys require high étendue (either large aperture mirrors and/or large field of view camera designs) and recent considerable progress in the development of large format CCD's are encouraging the construction of large aperture sky monitoring telescope facilities.

Table 4.1 compares the étendue of different existing and planned survey telescopes. In the near future, the Pan-STARRS survey and monitoring project will outperform existing asteroid and near-Earth object detection surveys like LINEAR and Spacewatch. In full operational mode, the Pan-STARRS program will ring in new standards in astronomical observations and image data processing. Results of data analysis will open a new window to the transient universe and reveal important insights into short-term astrophysical phenomena.

Telescope	$D(m)$	$A(m^2)$	$\Omega(deg^2)$	SP $(m^2 deg^2)$	observing status
UH 2.2m/PFCam	2.2	3.5	0.35	0.9	active
LINEAR	1.0	0.8	2	1.6	active
Spacewatch	0.9	0.6	3	1.8	active
CFTH/MegaCam	3.6	10	1	10	active
SkyMapper	1.35	5.7	8	46	2007 →
Pan-STARRS	3.6	10	7	70	2009 →
LSST	8.3	54	7	378	2012 →

Table 4.1: The survey power (SP) of various telescopes. D is the mirror diameter, A is the total collecting area and Ω is the field of view. The table is updated and reproduced from Jewitt (2003).

4.2 Limits on microlensing detection rate

Existing microlensing survey and monitoring projects (e.g. OGLE-III and MOA) are subject to practical constraints related to the telescope and detector system. As a consequence such monitoring programs have a number limited capability in detecting galactic microlensing events. Small aperture telescopes combined with narrow field CCD cameras have a natural upper bound in the detection rate of ongoing microlensing events.

The probability of detecting microlensing events increases within regions of high stellar surface densities. However, crowded fields suffer from object confusion and requires a good image quality (low seeing + high angular resolution over the entire CCD frame) for accurate photometry. In order to have a reasonable number of microlensing events which may show planet deviations, it is necessary to have i) $< 10\%$ accurate photometry at the $I \sim 19$ limiting magnitude, and ii) a high single-field monitoring cadence to detect the beginning/rise of an ongoing microlensing occurrence.

Monitoring programs with a too low cadence rate (or long field recurrence time) would inefficiently miss microlensing events for obvious reasons. For a typical Einstein-ring radius crossing time of 2 1/2 - 3 weeks, a sampling of only 1 to 3 data points during the initial magnification period is believed to be insufficient for a successful detection.

It is important to note that detecting transient microlensing events is hard. Classical variable phenomena, like eclipsing binaries, are recurrent and periodic in nature. The detection of these objects is still feasible under bad observing conditions. For an irregular sampling of observations of an regular-variable object, observations can be period phase folded in time in order to enhance the variability. In most cases this should reveal the binary periodic nature of the object. However, a microlensing event is a one-time event only. Its existence can only be determined by pointing the telescope at the right direction and start observations at the right moment.

Let A denote the total surveyed sky area and a the telescope field of view. Then

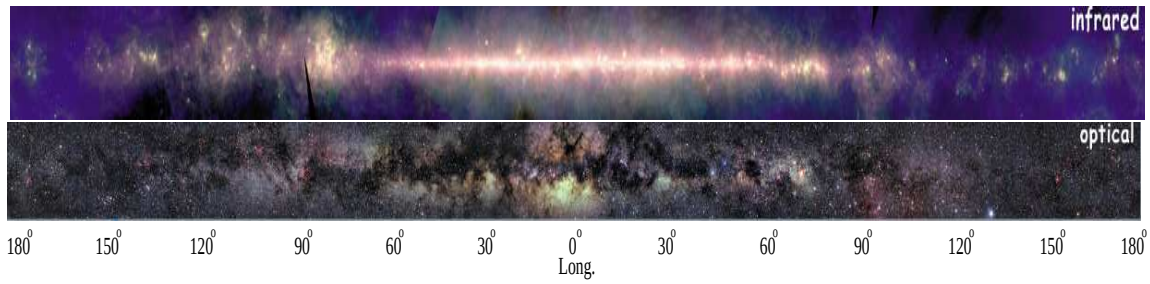

Figure 4.2: The Galactic plane within 10° in latitude as observed in different wavelength regions. *Upper panel*: Composite mid- and far infrared intensity map observed by the IRAS satellite in 12, 60 and 100 micron wavelength bands. Most of the emission is thermal, from interstellar dust warmed by absorbed starlight, including star-forming regions embedded in interstellar clouds. *Lower panel*: Intensity map of visible light of the Milky Way plane. Dark regions are due to absorbing clouds of dust and gas. The lower luminous patch at $(l, b) = (0°, 5°)$ is the Baades Window. A region unobscured by clouds allowing a direct sight to the Galactic center. Most of the OGLE-III survey fields cover this region (cf. with Fig. 3.1). Both figures are reproduced and taken from http://adc.gsfc.nasa.gov/mw. Both maps cover a total field of ~ 7200 deg.^{2} or equivalent to one-sixth of the total (4π sr.) sky.

the total number of fields is given by $N = A/a$. A too small field of view could result in a too high field recurrence time for a given survey area. However, if t_E and t_{ro} denotes the CCD exposure and readout time respectively, then the survey single field recurrence time is given by

$$T_s = \frac{1}{\tau} \times N \times (t_E + t_{ro}), \tag{4.2}$$

where τ is the observing duty-time (i.e fraction of time in which the telescope is in dedicated survey/monitoring mode). Increasing the duty-time would lower the field recurrence time leading to an increased sampling of each field per unit of time. In the following calculations, it is assumed that $\tau = 8/24$ on average.

To illustrate the ineligibility of existing (MOA and OGLE-III) and future (SkyMapper) monitoring programs to increase the total microlensing detection rate, different survey areas and their corresponding field recurrence times are compared. Table 4.2 shows field recurrence times for the OGLE-III, SkyMapper and MOA survey programs. Survey data for the Pan-STARRS project have been added for comparison.

The "super" surveys indicate the respective normal surveys with the exception of assuming that they are dedicated to scan the entire Galactic plane within 10° in latitude, corresponding to a total survey area of 7200 deg^2. In these survey scenarios identical telescope and hardware specifications are assumed.

From the table the survey field recurrence time for current ongoing monitoring programs spans from $T_s \sim 2.8$ days for OGLE-III to $T_s \sim 0.1$ days for MOA, depending on the respective survey area and camera field of view (both monitoring survey pro-

	$A\ (deg.^2)$	$a\ (deg.^2)$	N	$t_E\ (s)$	$t_{ro}\ (s)$	$T_s\ (days)$
Pan-STARRS (PS1)	30939	7	4420	30	10	6.2
"Super-Pan-STARRS"	7200	7	1029	30	10	1.4
OGLE-III	~ 90	0.336	268	200	100	2.8
"SUPER-OGLE-III"	7200	0.336	21429	200	100	226
SkyMapper	20000	5.7	3509	30	20	6.2
"SUPER-SkyMapper"	7200	5.7	1263	30	20	2.3
MOA	~ 50	2.2	23	100	20	0.1
"SUPER-MOA"	7200	2.2	3273	100	20	14
VYSOS	~ 25	0.3	83	240	20	0.8
"Super-VYSOS"	7200	0.3	24000	240	20	219

Table 4.2: Survey field recurrence times for various monitoring projects. "Super" surveys are hypothetical surveys, as if they are sheduled to monitor a 7200 deg.^{2} field of view of the Galactic disk using same telescope and camera equipment. Data for the MOA and VYSOS projects have been communicated by I.A.Bond and B. Reipurth.

grams cover less than 2% of the entire Galactic plane). Based on the current number of detected OGLE-III microlensing events within a given observing season (around 500 events, cf. Table 3.1), a 3-day field recurrence frequency appears to be sufficient for the detection of microlensing events. However, increasing the survey area to cover the 7200 deg.^{2} Galactic plane, increases the field recurrence time to $T_s \sim 226$ for the OGLE survey telescope hardware. Clearly, due to the small field of view, any given microlensing event would be missed in this scenario and monitoring setup.

Considering the most ideal case and utilising a hypothetical "super-Pan-STARRS" telescope facility within a dedicated all-Galactic plane microlensing survey and monitoring program, would be sufficient to detect a possible Jupiter-mass planet. However, a field recurrence time of $T_s = 1.4$ days, is still to long in order to certainly characterise (i.e model and extract physical parameters) a Jupiter-mass planet in orbit around the lensing host star (light-curve deviation introduced by a lensing Jupiter-mass planet is on the order of 1 day).

4.3 The VYSOS survey project

The VYSOS (Variable Young Stars Optical Survey) survey project aims at a systematic monitoring of near star forming regions within the Galactic plane (Reipurth et al., 2004). The VYSOS observing program is coordinated in a collaboration between the Institute of Astronomy (IfA) at the University of Hawaii and the Institute für Astronomie at the Ruhr-Universität Bochum. The main scientific objective is to study fundamental physical properties and characteristics related to early stellar evolution

by a continuous observation of young stars and their environmental surroundings.

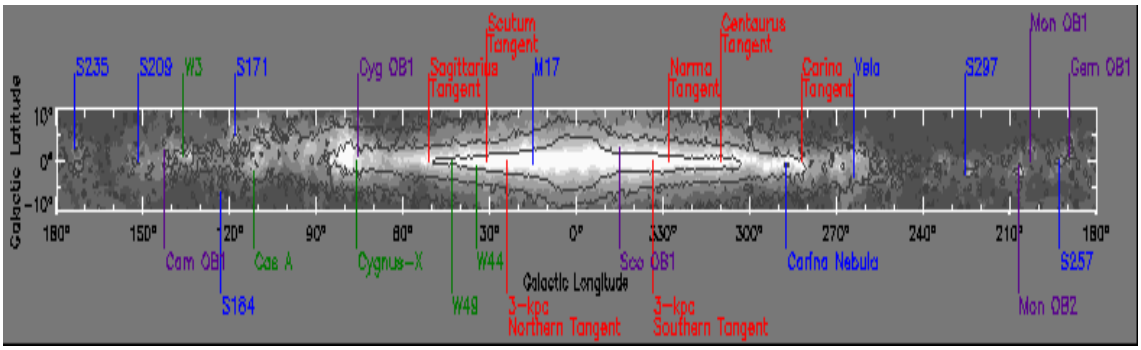

Figure 4.3: Major structures within the Milky Way. Main star forming regions are Cyg OB1, Carina Nebula, Gem OB1, Mon OB1 and Mon OB2. The Galactic disk plane is viewed within 10° in latitude. The central square region is the Galactic bulge. The entire area represents about one-sixth of the entire sky.

The survey is based on two identical robotic telescopes located in the northern (Haleakala Observatory, Hawaii) and southern (Cerro Pachón, Chile) hemisphere. Each telescope has an mirror aperture of 0.41m using a 2104×3117 pixel CCD camera with pixel scale 0.77"/pixel. The field of view is 27×40 arcmin (~ 0.3 deg^2). The telescope visual limiting magnitude of stellar objects is estimated to be around V = 19 mag at an estimated exposure time of 240 s (*private communication* B.Reipurth, Sept. 2006).

Currently, the telescopes are in a testing phase and continuous operation of monitoring/surveying star forming regions is expected by the end of 2006. Possible spin-off science with application to microlensing detections can be done using VYSOS photometry data. Image mosaics or CCD patches of particular high density stellar regions can be obtained from the original monitoring CCD field images and analysed for variability and transient phenomena. Contact to the VYSOS science team have been established (*private communication* with PI B.Reipurth, Sept. 2006) with a preliminary arrangement (by UGJ and TCH) on VYSOS data access and analysis for microlensing event search purposes.

4.4 The SkyMapper telescope

The SkyMapper telescope (http://www.mso.anu.edu.au/skymapper/index.php) will be utilised within the multi-colour, multi-epoch Stromlo Southern Sky Survey (SSS Survey) covering a total of 20000 deg^2 of the southern hemisphere. It is fully automatic and has a primary mirror aperture of 1.35m using a $16k \times 16k$ mosaic CCD camera with 0.5"/pixel covering a 6 deg^2 field of view. The telescope is located at Siding Spring

Observatory, Australia and currently under construction with first light expected to be in early 2007. 25% of the survey time will be dedicated to planet transit search and microlensing, wide-field survey studies. Data in form of calibrated photometric digital images will be made publicly available without a proprietary period within the Virtual Observatory facility (http://www.atnf.csiro.au/projects/avo/).

4.5 The Pan-STARRS monitoring project

A more advanced initiative is the Pan-STARRS (Panoramic Survey Telescope and Rapid Response System, http://www.pan-starrs.ifa.hawaii.edu/public/) survey and monitoring project. Pan-STARRS is operated by the University of Hawaii, Institute of Astronomy and utilises large scale cameras for a single site, wide-field imaging facility conducting astrometry and photometry observations of the sky with an unprecedented monitoring/survey frequency (Jewitt, 2003).

The primary goal of Pan-STARRS is devoted to the detection, identification and characterisation of potentially hazardous objects on possible impact collision course with Earth. Combining several small aperture telescopes with large format cameras will enable to scan the entire available sky (as visible from Hawaii which corresponds to three-quarters of the entire sky) several times within the dark lunar period. This rapid survey approach involves the generation and accumulation of static sky observations, producing a stream of difference images to reveal transient, variable or moving objects.

Celestial objects down to apparent (red)magnitude of 24 (or V = 16) are expected to be identified within single CCD images of 40 to 60 seconds of exposure time. Compared to the LINEAR asteroid search program, objects observed with the Pan-STARRS instrument are 5 times fainter in magnitude.

In full operational mode the Pan-STARRS project is a "array distributed aperture" observing facility, involving four identical telescopes (PS1 - PS4) on a single mount within a single enclosure dome. The array of telescopes all observe the same sky area simultaneously. The use of four identical telescopes enables to collect photons from each detector on a digital basis for image improvement purposes. This design setup identifies systematic errors like single CCD artifacts. Final locations for construction are being considered on both Mauna Kea and Haleakala, Hawaii.

Each telescope has a mirror aperture of 1.8 meter and is equipped with a 1.4 billion pixel camera, corresponding to a 3×3 degree field of view. The total light input is summed to produce the equivalent collecting area of a single 3.8 meter telescope. Each CCD camera is a 64 times 64 array of orthogonal transfer CCD's (OTCCD's have the same image stabilisation and correction effect like traditional "tip-tilt" adaptive optic systems) with each CCD component being approximately 600×600 pixels. Exposure times for faint objects down to limiting magnitude 24 are between 30 to 60 seconds. Data storage of each image corresponds to 2 Gigabytes. On average, the total amount

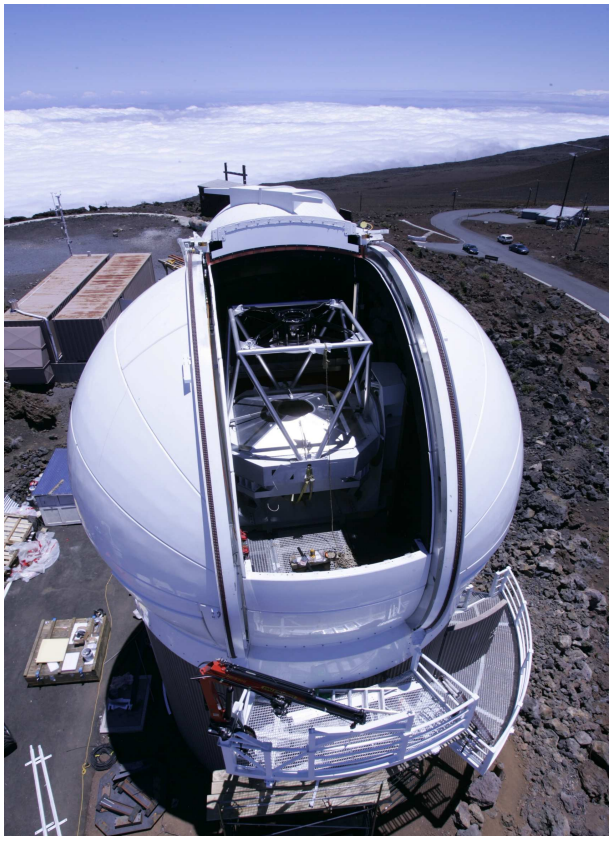

Figure 4.4: Image of the Pan-STARRS PS1 telescope on the summit of mount Haleakala (LURE Observatory, Maui), Hawaii. PS1 is only one of the four telescopes and is regarded as a prototype of the full Pan-STARRS system. PS1 will have same optics and camera design as the final system and allows to test the necessary technology (including data processing) that developed for the final system. The picture has been taking from http://pan-starrs.ifa.hawaii.edu/public/project-status/gallery.html and is reproduced with permission by the Pan-STARRS project, Institut for Astronomy, University of Hawaii.

of data during a single night corresponds to roughly 10 Terabyte of storage. The accumulation and processing of this huge data volume is unprecedented in current astronomical survey programs and will set new demands on computing hardware.

The first of the planned four 1.8m telescopes (PS1) is currently undergoing commissioning and first light were announced in June 2006 taking the first test images with a small provisional CCD camera. PS1 is considered as a Pan-STARRS prototype telescope constructed for testing purposes. Construction of PS1 has already completed at the summit of mount Haleakala, Maui. However, the full-size 1.4 billion pixel camera is still under development and a final system upgrade and assembly is expected in 2007. At this time the camera is considered to be the largest camera mounted on any

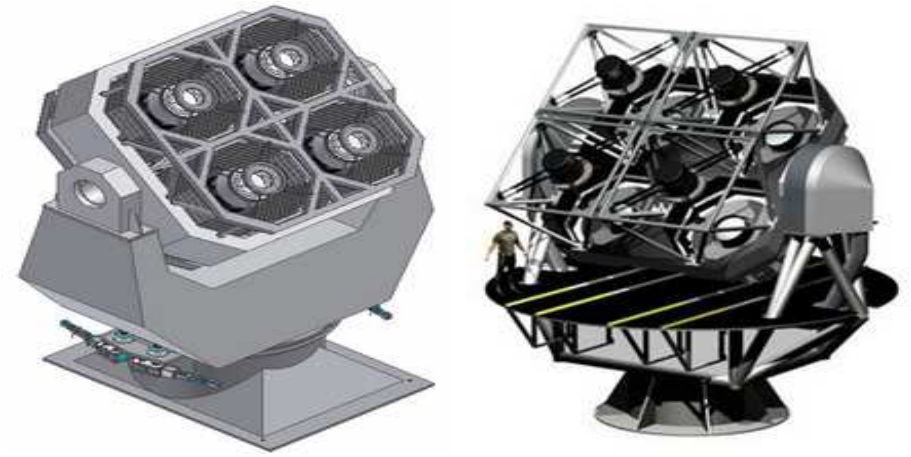

Figure 4.5: Two possible single mount designs of the full Pan-STARRS telescope array consisting of four 1.8m diameter mirrors. Individual telescope mounts are also considered as a possibility. The main feature of the Pan-STARRS telescope is its wide field imaging ability. Each telescope has its own 1.4 billion pixel camera and the field of view corresponds to six times the full diameter of the full moon. Site testing preferres the construction of Pan-STARRS at the mount Mauna Kea. The figures are taken from http://pan-starrs.ifa.hawaii.edu/public/project-status/gallery.html and reproduced with permission by Pan-STARRS, Institute for Astronomy, University of Hawaii.

ground-based telescope. The full four-mirror Pan-STARRS system is expected to be fully operational and on-line in 2009.

4.6 The LSST survey project

An even more ambitious project (compared to Pan-STARRS) is the Large Synoptic Survey Telescope (www.lsst.org) scheduled for first light in 2012 and currently in its initial design phase. In terms of étendue the LSST is a factor of five larger compared to the full Pan-STARRS system. According to the current LSST project baseline configuration, the observing facility is envisioned to be a large aperture, single mirror, wide-field imaging ground-based telescope (see Fig. 4.6). The main features for the LSST project is observational depth, rapid survey and continuous monitoring of the sky.

The LSST project will follow and even extend the Pan-STARRS paradigm shift of conducting astronomical observations and data handling in the 21st century. The science outlook by analysing LSST data covers almost every aspect in modern astrophysics research and opens a new window to the deep and transient universe. In particular, LSST observations will contribute to pursue open key scientific questions related to the solar system inventory and the formation of the universe itself.

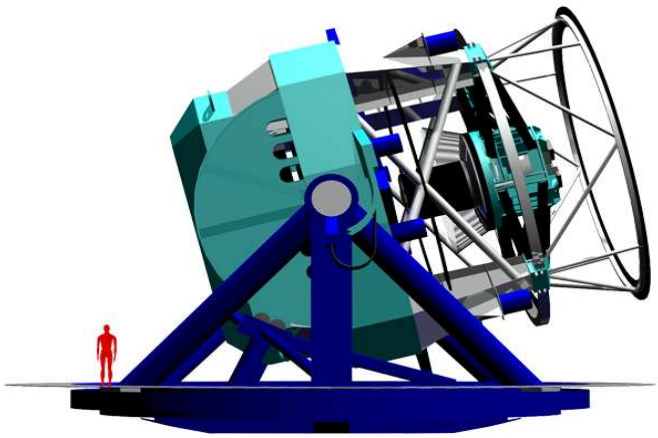

Figure 4.6: Preliminary conceptual design of the LSST survey and monitoring telescope. The construction is based on an Alt-Azimuth mount employing a 3-mirror modified Paul-Baker optical system representing a new telescope concept within observational astronomy. The deep curvature of the primary mirror results in a short focal length, providing the necessity of a compact and robust construction. The image is taken from www.lsst.org.

The optics design will consist of a 3-mirror system with an 8.4m wide primary mirror. The total field of view is anticipated to be 10 deg^2 (roughly corresponding to 50 times the area of the full moon) using a 3 billion pixel CCD camera. The nominal readout and exposure time will be 2 and 15 seconds, respectively. In full operation the LSST instrument will image 2000 deg^2 of the observable sky in 5 optical bands (300 - 1100 nm). The sky will be monitored and surveyed every 3 nights. The construction site for the LSST facility has been chosen to be Cerro Pachón - a $\sim$ 2500m high mountain peak in northern Chile.

Current astronomical data management needs to be revised and almost reinvented in order to store, process and analyse the huge LSST data stream. It is estimated that LSST will generate[1] 72 GB data every minute giving a data rate of 1200 MB pr. second!. At peak performance during a 10-hour winter night the LSST will produce a total of 30 TB (terabytes) of data. However, by the time the LSST telescope is in full operation, computing power is expected to comply the need of rapid data processing and analysis.

According to the LSST conceptual outline the primary goal of the LSST project is to make all data freely available to the end-user astronomer, amateurs and other potential users. *The LSST database will represent the largest non-proprietary data set in the world.* In the current LSST baseline configuration two main data products will

[1]For comparison, today's fastest astronomical data production rate is 4.3 MB/s generated within the Sloan Digital Sky Survey (SDSS)

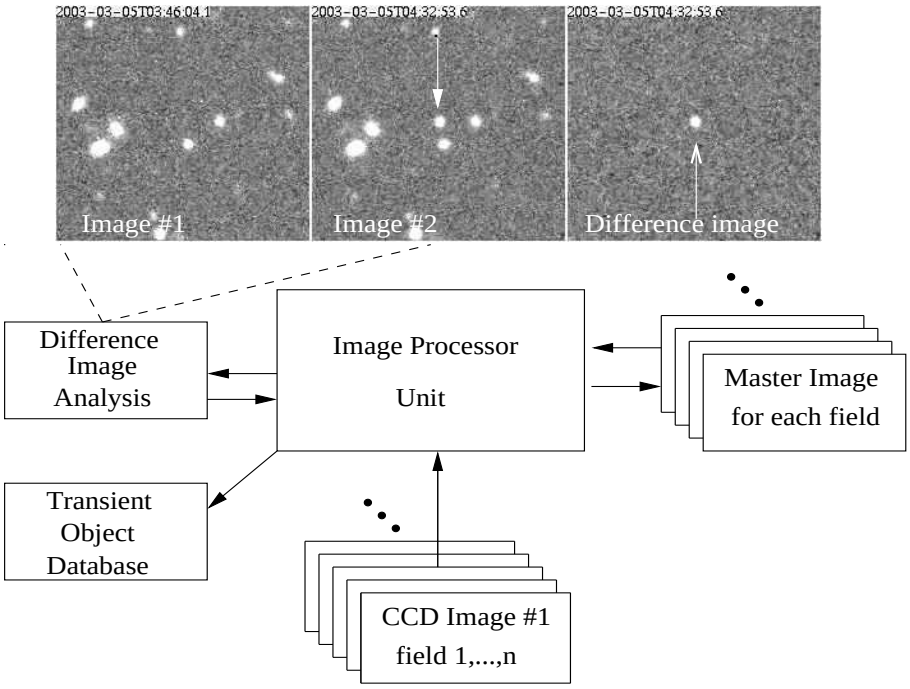

Figure 4.7: Outline of LSST data flow producing the two main data products. Obtained images are processed in the "Image Processor Unit". Images for each survey field are accumulated to form a single field master image. The master image will reveal faint objects of 27th magnitude. The collection of master images will provide a deep survey database of the available observed sky. The central processor will also generate difference images for the detection of variable, transient and moving objects - for the construction of a common database. Each raw CCD image will be deleted after successful analysis. In the figure, the difference CCD image shows the outburst of a supernova.

be made available to the scientific community: 1) the construction of a single database based on optimised LSST observations of variable/transient objects and 2) an in-depth map (including faint objects down to 27th magnitude) of the observable sky.

Chapter 5

Microlensing early-alert system

5.1 Introduction

The microlensing event detection rate depends on the number of observed stars within a given monitoring program. The probability of detecting a microlensing event is 10^{-6}. Consequently, to detect one lensing event the frequent monitoring of 10^6 stars is necessary.

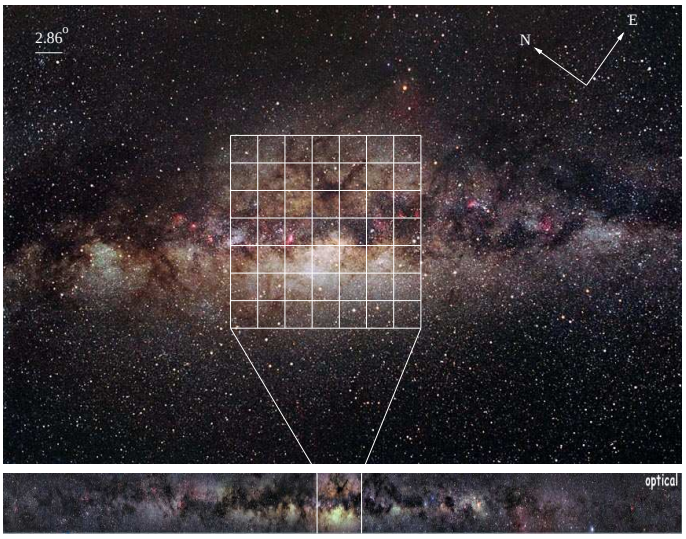

Figure 5.1: *Upper image*: Wide-angle view of the region around the Galactic bulge. Image field of view is approximately 47 × 70 degrees. The image is taken from www.guidescope.net/starfields/mw.htm and reproduced/edited with permission; courtesy T. G. Matheson (2006). The superimposed grid illustrates approximate field views for both Pan-STARRS and LSST images. Each box in the grid is 2.9 × 2.9 degrees. *Lower image*: The whole visible Galactic plane ($-10° \leq b \leq +10°$) and ($-180° \leq l \leq +180°$) is shown.

The detection of even more lensing event candidates is desirable and requires a constant monitoring of $10^7 - 10^8$ field stars. The detection probability increases the more high-density star fields are included within a given monitoring program.

Future survey and monitoring programs like Pan-STARRS and LSST will provide valuable photometric data enabling the opportunity to extensively search and detect microlensing events within the Galactic plane. Although the monitoring field recurrence frequency of these programs is high, they are still too low to extract and characterise a lensing planetary signal. Follow-up observations of promising lensing events (i.e high-magnification events) represents the final data acquisition step for a successful detection and characterisation of possible lensing extrasolar planets.

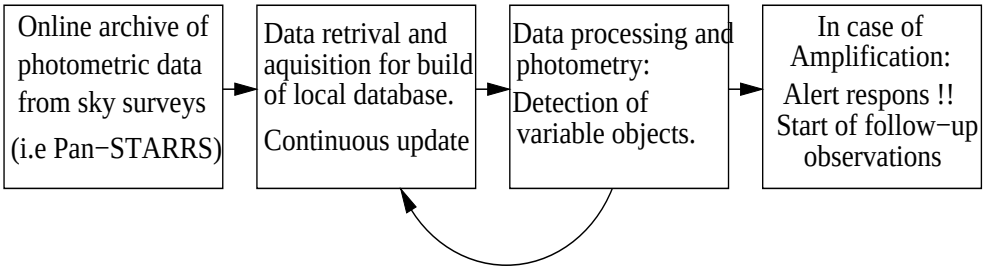

Figure 5.2: Basic steps in a data retrieval and analysis pipe line within the frame work of a microlensing early-alert system. Data processing of nightly images (step 3) is constantly compared with the photometric object data base (step 2). In case of a amplification the respective object is flagged and further analysed for reliability and likelihood. A possible follow-up observation of this object is then conducted.

An essential step towards a survey based early-alert system of microlensing detection is the development of *an automated data retrieval and analysis pipeline*. Retrieval of data will concentrate only on survey fields covering the Galactic plane. These fields are highly crowded and needs special analysis methods for extracting photometric information on transient and variable objects. The basic components of an automated data pipeline involves the following main steps:

1. Data (field image) download/retrieval from on-line monitoring data archive and subsequent image calibration/reduction.

2. Image processing and photometry by differential image analysis. This results in the creation of a photometry database of observed/monitored objects.

3. Search and detection of variable objects as images are retrieved in real-time.

5.2 Outline of an early-alert system

5.2.1 Data retrieval and analysis pipeline

A schematic layout of a data retrieval and analysis pipeline within the context of an automated microlensing detection and early-alert system is shown in Fig. 5.3. The pipeline is envisioned to process data in near real-time and starts by retrieving nightly images from a remote survey/monitoring data archive. Initial images will be used

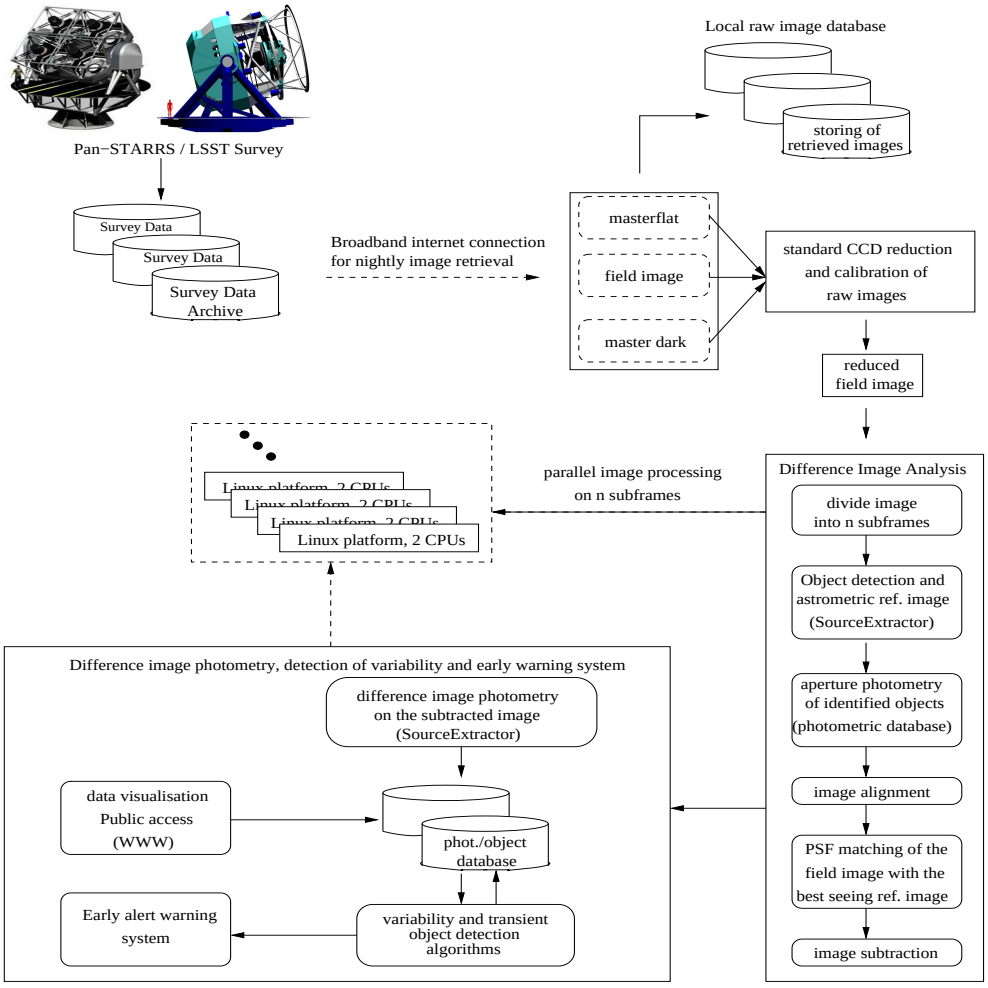

Figure 5.3: Schematic outline of an automated data retrieval and analysis pipeline within the frame work of a microlensing early alert system. The basic steps are straightforward involving the celebrated difference image analysis method for extracting photometry and variability of crowded field stellar objects. To speed up image processing the original image can be divided into n subframes and analysed on a multi-parallel CPU architecture.

to generate a master catalogue for each survey field. The master catalogue holds individual objects of interest and serves as a reference for future analysis.

Since the data generation of the survey is large, a dedicated broadband Internet connection is essential for ensuring real-time microlensing detections. Only star fields covering the Galactic plane will be considered within the retrieval process. Because the effect of gravitational lensing is wavelength independent, only one pass-band colour is needed for model analysis.

Depending on the exact form of the survey data product, calibration images (flat fields and dark images) are retrieved in addition for image reduction purposes. The retrieved raw images are then stored in a local image database archive. This ensures, if necessary, data availability for image re-analysis at a later time.

Processing and analysis of retrieved CCD images will rely on the *difference image analysis* method (Alard and Lupton, 1998; Alard, 2000). This method is close to optimal in detecting transient and variable objects within crowded fields and has found extensive use in on-going microlensing search surveys. By matching a nightly program image with a reference image of the same field, image subtraction will reveal any variations in brightness in form of a residual difference image.

Image photometry, object identification and classification is best done using the *SourceExtractor (SE) image analyis software* (Bertin and Arnouts, 1996). This method proofs effective for the fast processing of a huge volume of images. However, the processing speed of SE comes at the cost of photometry accuracy.

Increased accuracy can be obtained by using the widely used *stellar photometry package DAOPHOT* (Stetson, 1987; Stetson et al., 1990). This package is available within the IRAF programming environment and can be used on selected images in parallel. It is tailored for handling crowded field images and includes tasks like finding objects, aperture photometry, PSF determination and profile fitting photometry. Profile fitting in crowded fields is performed iteratively which improves the accuracy of the photometry for the image/object of interest.

Possible starting points for open source software packages for image analysis and photometry are at

1. www.astro.princeton.edu/∼wozniak/dia (OGLE pipeline)

2. http://www2.iap.fr/users/alard/ (difference image analysis)

5.2.2 Detection of a microlensing event

Because of limitations in ground based optical systems the determination of instrumental magnitude of a given object is associated with photometric inaccuracies. In order to detect and assess brightness variability a method is required to discriminate true variability from variability introduced by photometric measurement errors.

Within CCD photometry there exists three major noise sources: photon noise (also known as Poisson noise), background (or sky) noise, atmospheric scintillation noise and instrumental (systematic) noise. Hence, it is necessary to introduce an adequate definition of stellar non-variability. The following approach is heavily inspired by the work within (Udalski et al., 1993; Udalski, 1994; Udalski et al., 1994; Woźniak, 2000; Udalski, 2003).

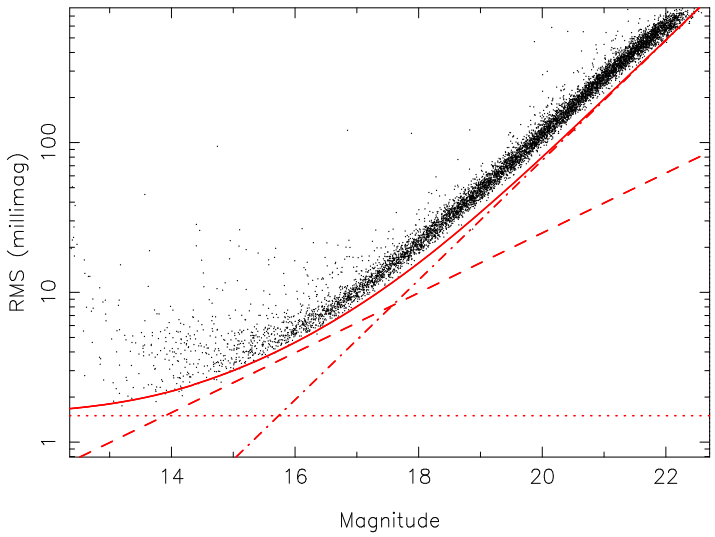

Figure 5.4: Example for a magnitude dispersion (RMS or σ) diagram for I-band observations of point-source stellar objects within the open cluster M34. The dashed line represents RMS contribution from Poisson (photon) noise. The dot-dashed line shows the RMS from sky (background) noise and the dotted line represents the RMS offset from systematic instrumental (read-out noise) RMS errors. Combining all noise sources together results in the predicted solid curve. The Figure is taken from Irwin et al. (2006).

To determine the variable nature of a given object with observed magnitude I, a magnitude dispersion diagram (or photometric precision diagram) is constructed for each monitored field. This diagram shows the photometric root mean square (RMS or σ) dispersion as a function of observed (V, I)-band magnitude (cf. Fig. 5.4). The dispersion (or time series dispersion) is calculated for each object identified within the field from time series photometry measurements and is given by

$$\sigma^2 = \frac{1}{N} \sum_{i=1}^{N} (I_i - \bar{I}), \tag{5.1}$$

where $\bar{I}$ is the average mean magnitude and N is the total number of photometric

measurements (cf. Fig. 3.2). Because of the finite light collecting mirror aperture of a telescope the RMS errors of faint stellar objects are larger and dominated by sky noise RMS contributions.

A magnitude dispersion diagram contains information on the distribution of the photometric time series RMS error as a function of I-band magnitude. As an example, Fig. 5.4 shows the observed light curve RMS distribution of stellar objects within M34 as determined by Irwin et al. (2006).

Within a given magnitude interval a RMS spread is observed for even bright stellar objects (I= $13^m - 16^m$). This scatter is explained by additional noise sources like variable stellar activity. Calculating the average dispersion of the RMS error within a given bin interval provides a measure of maximum allowed RMS error, σ_{max}. Single object photometric measurements with RMS error less than this maximum threshold can be considered as constant, non-variable objects. A functional fit through the σ_{max} points provides an analytic measure for the maximum allowed photometric spread as a function of I-band magnitude. This process requires the identification of variable stellar objects like eclipsing binaries or pulsar stars. A master catalogue of non-variable stars will then be generated in the course of data retrieval.

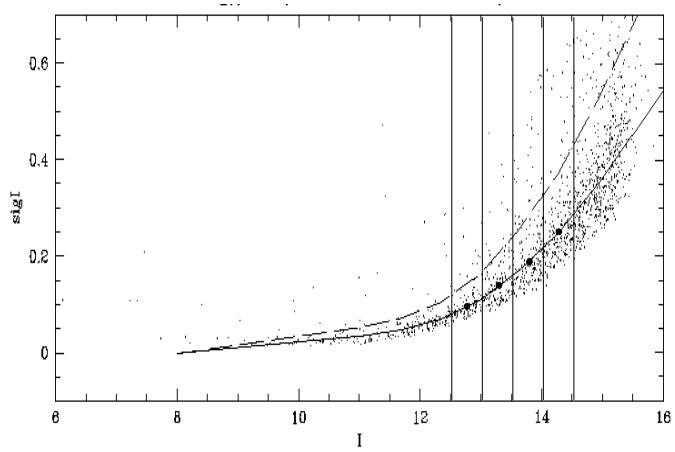

Figure 5.5: Magnitude dispersion diagram of a star field observed within the Pisgah Automated Survey (López-Morales and Clemens, 2004, Fig.10). The solid line is an exponential fit to the averaged σ (black dots) in 0.5 mag bins. The dashed line represents a 2σ deviation from the average solid line.

The main key point in a microlensing early-alert system is to constantly monitor the database of non-variable objects for a significant photometric deviation from the time series RMS magnitude. Udalski (1994) adopts a $3\sigma_{max}$ criterion for defining a significant photometric deviation. If a measurement for a given non-variable object is larger than three times the binned averaged magnitude dispersion, then this object is flagged as a potential microlensing event. To confirm a possible brightness change a total of 1-5

consecutive observations should stay above the 3σ level. The number of consecutive measurements is a trade-off between the number of false alarms and detection delay (Udalski, 1994) and possibly needs to be fine tuned for each star field.

5.3 Difference image analysis

5.3.1 PSF matching and image subtraction

A powerful method to detect variability in a series of CCD images is the difference image analysis (DIA) method developed by Alard and Lupton (1998). In its basic formulation this method aims to produce a residual image by subtracting two images observed at two consecutive times. In case of no variability the resulting difference image will show no residual offset against background pixels. However, if objects changes in brightness (or moves) any difference appears as a residual in the resulting difference image. The

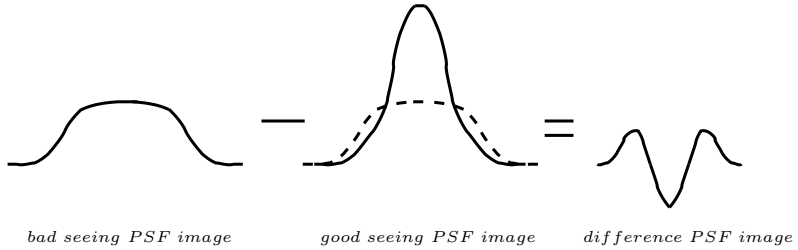

Figure 5.6: Illustration of subtracting two different PSFs representing two different observational seeing conditions of otherwise *two identical images*. The result is that too much is subtracted in the middle region and too little at the wings (the dashed line is shown for a direct comparison). This exemplifies the introduction of artificial residuals when the PSFs are not matched prior to subtraction. In order to match the PSF of both images the good seeing image needs to be degraded with a convolution kernel. This process only introduces loss in information representing the spread of accumulated light. The total amount of light is the constant. Details can be found in Alard and Lupton (1998).

process of subtracting one image from the other requires a PSF matching between the program image and a reference image of the same field. PSF matching between two images is crucial in order to avoid introducing artificial residuals indicating false variability. This point is illustrated in Fig. 5.6.

The PSF expresses *how* light from a point-source is distributed across the CCD detector. In terms of Fourier analysis this process is known as convolution and basically describes image (or point-source) degradation. The PSF can be decomposed into an instrumental and an atmospheric part. Within the matching process the good-seeing image PSF needs to be degraded to match the bad-seeing image. This requires the determination of a *convolution kernel*. Its effect is degrading the good-seeing image

PSF in order to match the bad-seeing image PSF. The kernel is to be determined by least squares analysis (Alard and Lupton, 1998).

In practice a photometric "master reference image" is constructed for each field by stacking several good-seeing images with possible low background noise. This reference image is used to subtract program images. In some cases the program image is of better photometric quality compared to the master reference image. Then the PSF degradation is performed on the program image.

The form of the PSF is subject to a turbulent time variable atmosphere. Within small field of view CCD exposures the PSF is unique for each stellar object in the image. For large format CCD field of views spatial variations of the PSF may occur across the CCD (since a larger patch of turbulent atmosphere is observed and assuming homogeneous turbulence is no longer valid). In this case a spatially varying convolution kernel needs to be determined (Alard, 2000).

The difference image contains only the variable part of the flux and can only be used for relative high precision photometry. Constructing a light curve in terms of magnitudes requires a zero point calibration. Photometric magnitudes are obtained by determine the flux of the star prior to the microlensing event.

An essential step in the difference image analysis is the geometric alignment of nightly images to an astrometric reference image (ARI) for a given field. This step is done before the PSF matching and subtraction process. Due to telescope pointing error, night-to-night images are different and star signals are therefore not centred on the same pixel positions. The process of PSF matching requires an exact alignment of all program images of the same field. The astrometric reference image is generated by stacking all available "best-seeing" images taken during the monitoring program. Nightly images are then eventually rotated or shifted to match the ARI by choosing a large number of high S/N stars as reference points.

5.3.2 Difference image photometry

Photometry on the residual difference image is best done using the SourceExtractor software as an essential part in the pipeline data flow. SExtractor (Bertin and Arnouts, 1996) automatically detects, deblends, measures and classifies objects in astronomical CCD images. It is very well suited to analyse large amounts of data with moderate to high photometric precision. Essentially, SExtractor completes 3 basic steps on each single CCD image:

1. Background estimation: In order to measure starfluxes accurately a precise estimate of the background is needed. In practice, SourceExtractor constructs a background map based on a user-defined grid of given mesh-size. Then the background image is subtracted from the calibrated image. However, since crowded fields are considered this background estimation might be a tricky process.

2. Find/detect objects and deblending (by thresholding): SE is using thresholding for the detection of objects in a given CCD image. A user-defined threshold limit is set from which SE starts to treat pixels to be object related. Pixels below the threshold are treated to belong to the background noise and are precluded in a subsequent source analysis. In a crowded CCD image objects are likely to overlap each other. This is known as source confusion or object blending. The separation between two objects (or deblending) is not always straightforward and needs special treatment. Within gravitational microlensing object deblending is a very important subject for a proper characterisation of the event parameters. In some cases object blending could even lead to the creation of an artificial lensing event. Under bad seeing conditions the point-spread function of objects starts to "smear out" possibly overlapping with adjacent point sources. Neighbouring pixels could then wrongly contribute to the total flux and hence falsely mimic a microlensing event.

3. PSF or aperture fitting photometry is then done for each identified variable object on the difference image. For a microlensing event, only the difference in flux is determined. The real flux change is derived from a mean flux as derived from previous time series measurements on retrieved images for a given object.

Chapter 6

SONG and microlensing follow-up observations

6.1 Introduction

The main difficulty in detecting planets using the microlensing method is the restricted access to existing observing facilities for continuous long-term observations. The presence of a microlensed planet is revealed by short-term deviations from the standard symmetric PSPL light curve. Because a lensing event is a one-time phenomenon only, it is crucial to continuously observe and sample the complete course of the event brightness variation.

Incomplete data in form of missing observations or poorly data sampling (with significant data gaps) of the lensing light curve renders the subsequent modelling process to be a difficult task and could result in ambiguous interpretations of the observations. Missing data in the microlensing light curve even have the potential of the non-detection of an otherwise existing lensing planet.

Ground based telescope networks dedicated for microlensing observations exist (e.g PLANET and MOA collaboration) as discussed in this report and a single space based mission is planned (Bennett and Rhie (2001)) for continuous follow-up observations in the near future. However, ground based follow-up microlensing observations could be improved by constructing additional central controlled small aperture telescope facilities. An interesting project is the SONG telescope network. Using identical small aperture telescopes located at different longitudes (different time zones) on the southern hemisphere this network represents an ideal setup for continuous high time-series photometry with a potential application to perform microlensing follow-up observations.

6.2 The SONG telescope network project

The SONG telescope network (http://astro.phys.au.dk/SONG/) is a Danish initiative to design and construct a global network of small ($\sim$ 1m class) telescopes. The current project envisions to install longitude distributed individual robotic telescopes around the globe (cf. left-hand panel in Fig. 6.1). Using existing observing sites for the network construction would lower the costs of expensive and tedious testing and experiment efforts. In addition, existing observatories have a well-developed infrastructure and their present locations are generally chosen because of excellent long-term weather conditions required for conducting reliable astronomical observations.

Currently, the SONG project is within a design and assessment study period. The SONG project time line estimates a start of operation of the network by late 2009. Development, construction and deployment activities of single network nodes are planned for the period 2007-2009.

With current advances in telescope and related instrument technology the realisation of the SONG project is highly realistic, feasible and scientifically competitive compared to other large-scale single site telescope facilities. In fact, such a network is highly demanded within the fields of asteroseismology and planet search, which relies on a uniform and continuous data acquisition process.

Figure 6.1: *Left panel*: Possible location of individual observing facilities within the planned SONG telescope network. For dedicated microlensing follow-up observations the southern node network is of particular interest during the Bulge season. *Right panel*: Possible outline of a single-site observing node. The figures have been taken from http://astro.phys.au.dk/SONG/.

In its final realisation, the SONG telescope network will represent a world-wide standalone and unique observing facility for continuous high-precision spectroscopy and photometry measurements. The use of identical observing instruments makes it manageable to identify and reduce systematic night-to-night observing errors. Apart from local weather influences on observing conditions on each site, the process of data merging from each individual site is in particular suitable and simple with the use of identical telescope hardware.

6.3 Planet detection with SONG

The main purpose of the SONG project is to establish a network of observing nodes dedicated for obtaining precise spectroscopic and photometric measurements. The scientific goals of the SONG project are *asteroseismology* and *planet detection*.

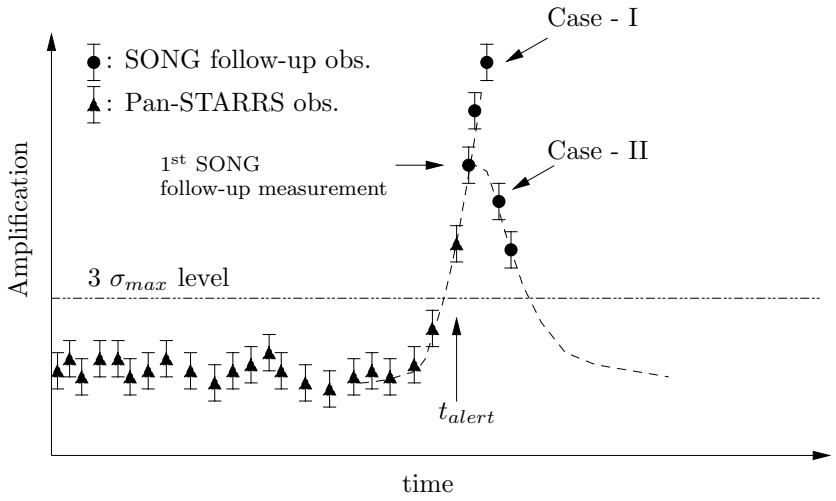

Figure 6.2: Schematic outline of a microlensing alert response for a single microlensed object. Retrieved large scale survey data are used to compile a database of non-variable stars within the Galactic field (denoted by ▲). The early-alert system is triggered (at time t_{alert}) as soon as one photometric data point deviates by more than 3 times the average time series RMS (3σ) for this star. A follow-up observation is then undertaken with the SONG network for confirming the deviation (denoted by •). Two possible scenarios are to be considered. (Case I) either the object is in the beginning of a microlensing rise or (Case II) the lensing event has almost been missed.

SONG observing nodes located on the southern hemisphere are of particular interest for planet detection within a microlensing follow-up observation programme. Ideal observing conditions are during the winter season on the southern hemisphere. In this period the galactic bulge is highest on the sky which preferably minimises observational seeing effects. By installing four longitude distributed and equally spaced single telescope sites, makes the night sky accessible to at least one telescope at any given moment. Apart from bad weather conditions the continuous observation of a single object (e.g an ongoing microlensing event) is then guaranteed by alternating between single network telescopes.

During a typical microlensing observing season each SONG telescope is provided with a microlensing target list for follow-up observations. The target list is compiled from detected on-going microlensing events using the microlensing early alert system based on data from large survey and monitoring programs. Target priority are given for microlensing candidates with a sufficient increase in brightness (i.e preference will

be given to high-magnification events). However, since the prediction of the maximum brightness is not a straightforward task the light curve of each monitored candidate will be reviewed on a regular basis and the list recompiled if necessary. Completed microlensing events will be withdrawn from the target list and new candidates considered for inclusion.

During a typical observing night a single SONG telescope will automatically cycle between on-going microlensing candidates according to the target list. Depending on target position and brightness, an optimal path for telescope slewing to the next object is required for maximum observing efficiency. After exposure each image is then uploaded to a central server for image analysis and quick target photometry determination. During the night, observations will accumulate and compile a real-time light curve for each individual lensing event. A light curve deviation algorithm will then monitor the progress of individual light curves and issues an alarm in case of detecting PSPL deviations. At the end of the night, target objects are to close to the horizon and the next network telescope will take over to warrant a smooth continuation of photometry data acquisition for current lensing events. In the ideal case, at the end of the observing night, photometry data are obtained from two nodes simultaneously. A major advantage of using a network of telescope nodes is the independent confirmation and coherent observations of a ongoing microlensing event.

Chapter 7

Summary and scientific outlook for Danish astronomy

7.1 Summary

The most promising observational technique available for the detection of solar system like extrasolar planetary systems is *gravitational microlensing*. The main advantage of this technique is its ability to *instantaneously* detect existing planets during a microlensing event. In particular, the microlensing technique is *sensitive to Earth-mass planets on Earth-like orbits*. Other techniques like radial velocity observations are still not sensitive enough to detect Earth-mass planets and otherwise rely on tedious constant monitoring over long period of times in order to extract and confirm the presence of a wide orbit Jupiter-mass planet.

Although gravitational microlensing provides an almost immediate detection of possible lensing planets, it only contributes with statistical data on the mass ratio, orbital separation and the frequency of extrasolar planets. This is opposed to the radial velocity technique providing a geometric picture of the system inventory and planet properties. However, both techniques complement each other and contribute with observational constrains to adjust current and future planet formation theories.

An interesting aspect in the technique of gravitational microlensing is the potential of extracting valuable information of possible lensing planets during *high-magnification* lensing events. In these events the probability of detecting a lensing planet increases dramatically disregarding the underlying orbit geometry. Numerical simulations assess that Earth-like planets are detectable within 1.5 - 2.5 AU and Jupiter and Neptune-mass planets within 10 AU. An important point to stress is the important science implications in the case of an *unsuccessful detection* of a planetary signal during a high-magnification event. The observed absence of a planetary signal allows an exclusion with high confidence of existing lensing planets over a large range of orbital radii.

Observing several planet-missing high-magnification events places upper bounds on the abundance of planets within the population of stars within our Galaxy.

The basis of detecting lensing planets is provided by microlensing surveys. The majority of microlensing events are detected and announced in near real-time within the pioneering OGLE and MOA survey projects. Selected events are then targeted for subsequent continuous follow-up observations with dedicated high time sampling observations of promising candidates. Intensive follow-up observations within the PLANET collaboration detected and characterised the first Earth-like planet involving Danish observing participation.

By investing efforts in the design and development of a data retrieval and analysis pipeline based on large format sky survey and monitoring programmes will provide an increasing number of detected microlensing events within the Galactic plane. Taking advantage of non-proprietary photometric data from the very beginning, enables potential spin-off science projects related to different astrophysics research disciplines.

A microlensing early alert system based on future survey and monitoring programs will find tailored application within the Danish initiated SONG project. The SONG observing network represents a unique opportunity to conduct near ideal microlensing follow-up observations. Longitude distributed network nodes of automated telescopes ensures the continuous and dense observation of ongoing lensing events. Deploying identical observing facilities provides homogeneous acquisition of photometric data providing an ideal condition for the subsequent data modelling and analysis process.

Using high-resolution spectrographs SONG observing facilities are envisioned to accurately measure stellar oscillation frequencies of nearby stars. Fourier analysis of continues long-term spectral observations, will be able to extract a signal attributable to a terrestrial-mass planets orbiting around the host star in orbits complementary of what is possible with the microlensing technique.

7.2 Science applications for Danish astronomy

A data retrieval and analysis pipeline as outlined in this report provides valuable access to additional spin-off science to be conducted within the Danish astrophysical research community. Pipeline software development could be undertaken within a collaboration involving Danish astrophysical science centres and participating international research institutes. The realisation of this conception would promote Danish astrophysics science research activity at a high competitive level and provide additional educational outlook with potential teaching applications.

The aggregated database could be mined and analysed for supplementary variability search projects and the database could be extended to contain multi-colour photometry data. Different survey fields could be retrieved to construct additional project oriented databases for further analysis and mining. Possible science applications of the pipeline

could be

1. supernova searches.
2. detection of gamma-ray bursts.
3. cepheids surveys in other galaxies.
4. pulsar variables.
5. variable binary stars.
6. transit search of extrasolar "hot Jupiter" planets.
7. extragalactic gravitational lensing.

The pipeline should be designed to be easily extended or modified to comply with requirements of specific variability search projects. Essentially the implementation of automatic variability search and classification algorithms are necessary within the variability detection stage of the pipeline.

Acknowledgements

We are grateful to IDA (Instrumentcenter for Danish Astrophysics) for financial support making this report possible. We are also thankful to I.A. Bond, B. L. Jensen, J. de Jong, B. Reipurth and A. Udalski for helpful comments and advice on specific aspects presented in the report.

Bibliography

Abe, F. et al.: 2004, *Search for low-Mass Exoplanets by Gravitational Microlensing at high magnification*, *Science* **305**, 1246

Alard, C.: 2000, *Image subtraction using a space-varying kernel*, *Astron. Astrophys. Suppl. Ser.* **144**, 363

Alard, C. and Lupton, R.: 1998, *A method for optimal image subtraction*, *ApJ* **503**, 325

Alcock, C. et al.: 2000, *The Macho Project: Microlensing optical depth towards the Galactic Bulge from difference image analysis*, *ApJ* **541**, 734

Beaulieu, J.-P. et al.: 2006, *Discovery of a cool planet of 5.5 Earth masses through gravitational microlensing*, *Nature* **439**, 437

Bennett, D. and Rhie, S. H.: 2001, in *ASP Conf. Ser. 239: Microlensing 2000: A New Era of Microlensing Astrophysics*, pp 393–+

Bennett, D. P. and Rhie, S. H.: 1996, *Detecting Earth-mass planets with gravitational microlensing*, *ApJ* **472**, 660

Bertin, E. and Arnouts, S.: 1996, *SExtractor: Software for source extraction*, *A&A Suppl.* **117**, 393

Bond, I. et al.: 2002, *Improving the prospects for detecting extrasolar planets in gravitational microlensing events in 2002*, *Mon. Not. R. Astron. Soc.* **311**, L19

Bond, I. A. et al.: 2004, *OGLE 2003-BLG-235/MOA 2003-BLG-53: A planetary microlensing event*, *Astrophys. J.* **606**, L155

Chung, S.-J. et al.: 2005, *Properties of central caustic s in planetary microlensing*, *ApJ* **630**, 535

Djorgovski, S. et al.: 2000, *Exploration of large digital sky surveys*, *astro-ph/0012489*

Dong, S. et al.: 2006, *Planetary detection efficiency of the magnification 3000 microlensing event OGLE-2004-BLG-343*, *ApJ* **642**, 842

Gould, A. et al.: 2006, *Microlens OGLE-2005-BLG-169 Implies That Cool Neptune-like Planets Are Common*, *ApJL* **644**, L37

Gould, A. and Loeb, A.: 1992, *Discovering Planetary Systems through gravitational microlensing*, *ApJ* **396**, 104

Griest, K. and Safizadeh, N.: 1998, *The use of high-magnification microlensing events in discovering extrasolar planet*, *ApJ* **500**, 37

Hearnshaw, J. B. et al.: 2005, *The MOA 1.8-metre atl-az wide-field survey telescope and the MOA project*, *astro-ph/0509420v1*

Irwin, J. et al.: 2006, *The Monitor project: rotation of low-mass stars in the open cluster M34*, *MNRAS* **370**, 954

Jewitt, D.: 2003, *Project Pan-STARRS and the Outer Solar System*, *Earth, Moon and Planets* **92**, 465

López-Morales, M. and Clemens, J.: 2004, *The Pisgah Automated Survey: A photometric Search for Low-Mass Detached Eclipsing Binaries and Other Variable Stars*, *PASP* **116**, 22

Lynds, R. and Petrosian, V.: 1989, *Luminous Arcs in Clusters of Galaxies*, *Astrophys. J.* **336**, 1

Mahabal, A. et al.: 2004, *Time domain explorations with digital sky surveys*, *astro-ph/0412164*

Mao, S.: 2001, *Gravitational Microlensing: Past, Present, and Future*, *ASP Conf. Ser. 237: Gravitational Lensing: Recent Progress and Future Goals* p. 215

Mao, S. and Paczyński, B.: 1991, *Gravitational Microlensing by double stars and planetary systems*, *ApJ* **347**, L37

Mayor, M. and Queloz, D.: 1995, *A Jupiter-mass Companion to a Solar Type Star*, *Nature* **378**, 255

Nemiroff, R. and Rafert, J.: 1999, *Toward a continuous record of the sky*, *PASP* **111**, 886

Paczyński, B.: 1986a, *Gravitational Microlensing at Large Optical Depth*, *Astrophys. J.* **301**, 503

Paczyński, B.: 1986b, *Gravitational Microlensing by the Galactic Halo*, *Astrophys. J.* **304**, 1

Paczyński, B.: 1996, *Gravitational Microlensing in the Local Group*, *Annu. Rev. Astron. Astrophys.* **34**, 419

Perryman, M.: 2000, *Extrasolar planets*, *Rep.Prog.Phys.* **63**, 1209

Rattenbury, N. et al.: 2002, *Planetary microlensing at high magnification*, *Mon. Not. R. Astron. Soc.* **335**, 159

Reipurth, B., Chini, R., and Lemke, R.: 2004, *The VYSOS robotic telescope project*, *AN* **325**, No. 6

Roulet, E. and Mollerach, S.: 1997, *Microlensing*, *Physics Reports* **279**, 67

Stetson, P. B.: 1987, *DAOPHOT - A computer program for crowded-field stellar photometry*, *PASP* **99**, 191

Stetson, P. B., Davis, L. E., and Crabtree, D. R.: 1990, *Future development of the DAOPHOT crowded-field photometry package*, *ASP Conf. Ser. 8: CCDs in astronomy* pp 289–304

Udalski, A.: 1994, *The Optical Gravitational Lensing Experiment: The Early Warning System. Real Time Microlensing*, *Acta Astron.* **44**, 227

Udalski, A.: 2003, *The Optical Gravitational Lensing Experiment: Real Time Data Analysis in the OGLE-III survey*, *Acta Astron.* **53**, 291

Udalski, A. et al.: 1993, *The Optical Gravitational Lensing Experiment Color-Magnitude Diagrams of the Galactic Bulge*, *Acta Astron.* **43**, 69

Udalski, A. et al.: 1994, *The Optical Gravitational Lensing Experiment: The Optical Depth to Gravitational Microlensing in the Direction of the Galactic Bulge*, *Acta Astron.* **44**, 165

Udalski, A. et al.: 2005, *A Jovian-Mass Planet in Microlensing Event OGLE-2005-BLG-071*, *ApJL* **628**, L109

Woźniak, P.: 2000, *Difference Image Analysis of the OGLE-II Bulge Data I. The Method*, *Acta Astron.* **50**, 421